

Dissecting CLIP: Decomposition with a Schur Complement-based Approach

Azim Ospanov*, Mohammad Jalali†, Farzan Farnia‡

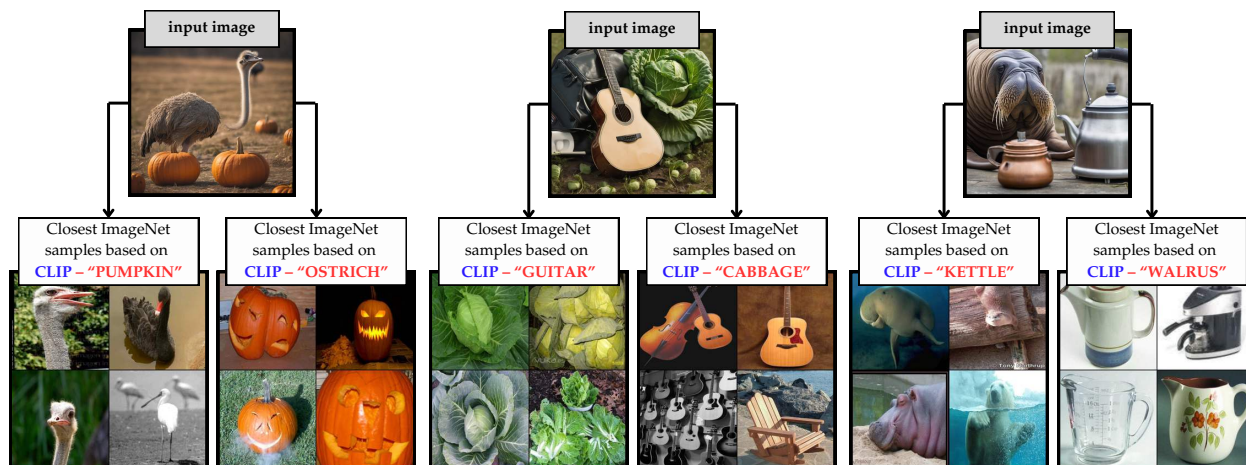


Figure 1: An example of the CLIP embedding decomposition. The top row features images composed of two distinct concepts, such as "pumpkin" and "ostrich." In the bottom row, the top four ImageNet images with the highest CLIP scores are displayed after the specified concept has been removed from the embedding.

Abstract

The use of CLIP embeddings to assess the alignment of samples produced by text-to-image generative models has been extensively explored in the literature. While the widely adopted CLIPScore, derived from the cosine similarity of text and image embeddings, effectively measures the relevance of a generated image, it does not quantify the diversity of images generated by a text-to-image model. In this work, we extend the application of CLIP embeddings to quantify and interpret the intrinsic diversity of text-to-image models, which is responsible for generating diverse images from similar text prompts. To achieve this, we propose a decomposition of the CLIP-based kernel covariance matrix of image data into text-based and non-text-based components. Using the Schur complement of the joint image-text kernel covariance matrix, we perform this decomposition and define the matrix-based entropy of the decomposed component as the *Schur Complement Entropy (SCE)* score, a measure of the intrinsic diversity of a text-to-image model based on data collected with varying text prompts. Additionally, we demonstrate the use of the Schur complement-based decomposition to nullify the influence of a given prompt in the CLIP embedding of an image, enabling focus or defocus of embeddings on specific objects or properties for downstream tasks. We present several numerical results that apply our Schur complement-based approach to evaluate text-to-image models and modify CLIP image embeddings. The codebase is available at <https://github.com/aziksh-ospanov/CLIP-DISSECTION>

*Department of Computer Science and Engineering, The Chinese University of Hong Kong, aospanov9@cse.cuhk.edu.hk

†Department of Computer Science and Engineering, The Chinese University of Hong Kong, mjalali24@cse.cuhk.edu.hk

‡Department of Computer Science and Engineering, The Chinese University of Hong Kong, farnia@cse.cuhk.edu.hk



Figure 2: Comparison of model-driven (left) and prompt-driven (right) diversity in 200 images generated for similar "cat and dog" prompts (left) vs. 200 images generated for diverse "cat and dog" prompts (right). While unconditional metrics favor the right-side case, the SCE score isolates intrinsic model diversity, suggesting greater model diversity on the left.

1 Introduction

Text-based generative models, which generate samples guided by input text, have gained significant attention in computer vision research. In particular, text-to-image models, which create images based on input text, have found numerous applications and are widely used across various content creation tasks. Given the important role of text-to-image models in many AI applications, their training and evaluation have been extensively studied in recent years. A comprehensive evaluation of these models, addressing relevance, diversity, and fidelity, is essential to ensure their effectiveness and adaptability across different use cases.

As the CLIP model [1] provides a joint embedding for text and image data, CLIP embeddings have been widely used to evaluate and interpret the performance of text-to-image models. By calculating the cosine similarity between the CLIP embeddings of text and image data, the CLIPScore [2] serves as a metric for measuring the alignment between the text and the generated image. While the CLIPScore and similar uses of CLIP embeddings focus on evaluating the fidelity and relevance of generated samples, these embeddings have not yet been applied to assess the diversity of data produced by text-to-image models. Existing evaluation frameworks typically address diversity scores for unconditional generative models, such as Recall [3, 4], Coverage [5], and Vendi [6], which assess image samples independently of the input text.

However, the diversity of images generated by a text-to-image model depends both on the variety of input text data and on the model's intrinsic diversity, which produces different images in response to similar prompts. Consequently, existing diversity metrics for unconditional generative models cannot differentiate between diversity arising from varied prompts and diversity contributed by the model itself. In this work, we leverage CLIP embeddings to propose a framework for quantifying and interpreting the intrinsic diversity of both text-to-image and image captioning (image-to-text) models. The primary objective of our approach is to decompose the CLIP image embedding into a text-based component, influenced by the input text, and a non-text-based component, arising from the model's inherent randomness.

To achieve this goal, we employ a kernel similarity function and focus on the kernel covariance matrix for the generated (text, image) pairs. Using a Gaussian elimination-based approach in a proper kernel space, we decompose the image sub-covariance matrix, C_{II} , into the sum of the Schur complement component, $C_{II} - C_{IT}C_{TT}^{-1}C_{TI}$, which represents the model-driven diversity component, and the remainder term $C_{IT}C_{TT}^{-1}C_{TI}$, which captures the prompt-driven variety in the generated images. Leveraging the estimated kernel covariance matrices from generated data, we define the matrix-based entropy of the Schur complement component, as *Schur Complement Entropy (SCE)*, as a measure of model-driven diversity in the generated images.

To illustrate the effectiveness of the SCE score in distinguishing model-driven diversity from prompt-driven effects, we present a comparative example. Figure 2 compares the SCE-Image model diversity scores for

samples generated by DALL-E 3 [7]. The left-side subfigure represents model-driven diversity, showing images of diverse-breed cats and dogs generated using similar prompts like “cat and dog read a text.” The right-side subfigure illustrates prompt-driven diversity, featuring same-breed cats and dogs across diverse-occasion prompts. While unconditional diversity metrics such as Vendi and RKE report higher diversity for the right-side case, the SCE score, designed to isolate intrinsic model diversity from prompt-driven effects, indicates greater diversity in the left-side case. This example highlights the advantage of the prompt-conditioned SCE score over existing unconditional diversity metrics.

We present several numerical applications of the proposed framework to evaluate and interpret standard text-to-image and image-captioning models. Our results on several simulated scenarios with known ground-truth diversity indicate that the proposed entropy metric correlates with the non-text-based diversity in images, capturing variation not attributable to the text prompt. Additionally, we show that the decomposed feature component can neutralize the influence of specific objects in the text prompt within the image embedding. Specifically, we use this decomposed feature to diminish the impact of visible text in images, reducing its effect on the embedding. We also demonstrate how the decomposed image embedding can enhance or reduce the focus on particular objects or styles within an image, which can have implications for downstream applications of CLIP embeddings when emphasizing specific elements. For instance, Figure 1 shows a generated image of an ostrich next to a pumpkin. We demonstrate the ImageNet samples with highest CLIPScore to the original image embedding and to the modified image embedding when subtracting the Schur complement-method embedding after canceling texts "pumpkin" and "ostrich", which shows the modified embedding removes the effect of the unwanted object. The main contributions of this work are summarized as follows:

- Proposing a Schur Complement-based approach to text-to-image diversity evaluation that decomposes the diversity metric into prompt-induced and model-induced components
- Providing a decomposition method that allows to remove directions from the CLIP embedding based on the Schur Complement modified image embedding
- Presenting numerical results on the Schur complement-based decomposition of CLIP embeddings

2 Related Work

CLIP interpretability and decomposition. Contrastive vision-and-language models, such as CLIP [1] are a class of models that were trained on paired text prompts and images. The notable feature of CLIP is a shared embedding space between image and text data. A common interpretability method involves heatmaps to highlight relevant image areas [8–10]. However, heatmaps are used to identify objects and lack spatially dependent information, such as object size and embedding output. Other approaches require decomposing the model architecture and analyzing attention heads. [11] introduced *TextSpan*, which finds a vector direction for each attention head and assigns it an appropriate text label. Another prominent approach, proposed in [12], decomposes dense CLIP embeddings into sparse, interpretable semantic concepts to enhance embedding description. [13] suggests disentangling written words from underlying concepts via orthogonal projection of learned CLIP representations.

Evaluation of Diversity in Generative Models. Diversity evaluation in generative models has been extensively explored in the literature, with existing metrics broadly classified as either reference-based or reference-free. Reference-based metrics, such as FID [14], KID [15], and IS [16], assess diversity by quantifying the distance between true and generated data. Metrics like Density and Coverage [5], and Precision and Recall [4] evaluate quality and diversity by analyzing the data manifold. Reference-free metrics, including Vendi [6, 17], RKE [18], and their variations like Nyström-Vendi and FKEA-Vendi [19], measure the entropy of a similarity metric (e.g., kernel matrix), capturing the number of distinct modes in the data. Since these metrics do not require a reference distribution, they are particularly suitable for text-to-image model evaluation, where selecting an appropriate reference dataset is challenging.

Evaluation of Text-to-Image Generative Models. Conditional generation models have been extensively studied, with CLIPScore [2] and its variations, such as Heterogeneous CLIPScore [20], being the standard metrics for assessing prompt-image alignment using cosine similarity. Another key approach is the FID framework adapted for conditional models, which measures the joint distribution distance between prompts and images, known as FJD [21]. Holistic evaluation methods, such as the HEIM [22] and HELM [23] benchmarks, unify different aspects of generated data to provide comprehensive assessments. Diversity evaluation typically involves generating multiple images per prompt and measuring their inter-diversity [24, 25]. Existing metrics require redundant image generation for diversity measurement, whereas our proposed Schur Complement-based decomposition bypasses this need, enabling evaluation on pre-generated datasets without requiring multiple images per prompt.

3 Preliminaries

Kernel Functions. We call $k : \mathcal{X} \times \mathcal{X} \rightarrow \mathbb{R}$ a kernel function if for samples $x_1, \dots, x_n \in \mathcal{X}$, the resultant kernel matrix $K = [k(x_i, x_j)]_{1 \leq i, j \leq n}$ is a PSD (positive semi-definite) matrix. Moreover, K can be decomposed into a dot product of feature maps ϕ , referred to as the kernel trick, as follows:

$$k(x, x') = \langle \phi(x), \phi(x') \rangle \quad (1)$$

In this work, we provide several numerical results for the cosine-similarity Kernel function defined as:

$$k_{\text{Cosine-Similarity}}(x, x') := \frac{\langle x, x' \rangle}{\|x\|_2 \|x'\|_2} \quad (2)$$

In our numerical analysis, we also consider the Gaussian Kernel defined as:

$$k_{\text{Gaussian}(\sigma)}(x, x') := \exp\left(-\frac{\|x - x'\|_2^2}{2\sigma^2}\right) \quad (3)$$

Note that both of the presented kernels are normalized kernels, since the self-kernel similarity $k(x, x) = 1$ for every $x \in \mathcal{X}$. In order to apply entropy measures, we consider the normalized kernel matrix given by $\frac{1}{n}K$. Therefore, we observe $\text{Tr}(\frac{1}{n}K) = 1$ for every normalized kernel, implying that the eigenvalues of $\frac{1}{n}K$ form a probability measure, as they are non-negative and sum up to 1.

Matrix-based Entropy and Kernel Covariance Matrix. Given a PSD matrix A with unit trace and eigenvalues $\lambda_1, \dots, \lambda_n \geq 0$, the Von-Neumann entropy is defined as:

$$H(A) := \text{Tr}(-A \log A) = \sum_{i=1}^n \lambda_i \log \frac{1}{\lambda_i}, \quad (4)$$

where $\text{Tr}(\cdot)$ denotes the matrix trace. As demonstrated in quantum information theory, the Von Neumann entropy measures the spread of eigenvalues. [6, 18] show that it can effectively count the number of sample clusters in the collected data. As noted by [6, 18], $\frac{1}{n}K$ shares the same non-zero eigenvalues with the kernel covariance matrix $\widehat{C}_{\mathcal{X}}$ defined as:

$$\widehat{C}_{\mathcal{X}} := \frac{1}{n} \sum_{i=1}^n \phi(x_i) \phi(x_i)^\top = \frac{1}{n} \Phi^\top \Phi \quad (5)$$

where $\Phi \in \mathbb{R}^{n \times d}$ is an $n \times d$ matrix whose rows are the feature presentations of samples $\phi(x_1), \dots, \phi(x_n)$. Feature representation varies between kernel methods. In Cosine Similarity Kernel, $\phi(x) = \text{CLIP}(x) / \|\text{CLIP}(x)\|_2$, i.e. normalized CLIP embedding of sample x , whereas in shift-invariant kernels, ϕ is a proxy feature map of the Gaussian kernel following the random Fourier features [26].

Schur Complement. Consider a block matrix Λ with a symmetric matrix partition as follows:

$$\Lambda = \begin{bmatrix} B & C \\ C^T & D \end{bmatrix}$$

where B and D are square symmetric submatrices. If B is invertible, the Schur Complement of B in A is given by $S = D - C^T B^{-1} C$. In general, even if B is not invertible, B^{-1} can be replaced with the Moore-Penrose pseudoinverse B^\dagger in the Schur complement definition. Note that the Schur complement $S \succeq \mathbf{0}$ will be PSD for a PSD matrix $\Lambda \succeq \mathbf{0}$.

4 Diversity Evaluation for Text-to-Image Generative Models via CLIP Embedding

As discussed earlier, the CLIP model offers a joint embedding of text and image data, which enables defining joint (text,image) kernel covariance matrices for the collected data. Suppose that we have collected n paired text,image samples (T_j, I_j) for $j = 1, \dots, n$. Here I_j represents the j th image and T_j represents the corresponding text. The application of CLIP embedding transfers the pair to the share embedding space \mathcal{X} and results in embedded samples (x_{T_j}, x_{I_j}) in the CLIP space. As a consequence of the joint embedding, not only can we compute the kernel function between (text,text) and (image,image) pairs, but also we can compute the kernel function for a (text,image) input.

To analyze the embedded sample, consider a kernel function $k : \mathcal{X} \times \mathcal{X} \rightarrow \mathbb{R}$ with feature map $\phi : \mathcal{X} \rightarrow \mathbb{R}^d$ where \mathcal{X} is the CLIP space and d is the dimension of the kernel feature map. Then, for the collected samples, we define the embedded image feature matrix $\Phi_I \in \mathbb{R}^{n \times d}$ whose j th row is $\phi(x_{I_j})$ for the j th image. Similarly, we define the embedded text feature matrix $\Phi_T \in \mathbb{R}^{n \times d}$ for the text samples. Note that the resulting CLIP-based kernel covariance matrix for the joint (text,image) map $[\phi(\mathbf{x}_T), \phi(\mathbf{x}_I)]$ is

$$C_{\text{joint (I,T)}} := \begin{bmatrix} C_{II} & C_{IT} \\ C_{IT}^\top & C_{TT} \end{bmatrix}$$

In the above, we define the sub-covariances as follows:

$$C_{II} = \frac{1}{n} \Phi_I^\top \Phi_I, C_{IT} = \frac{1}{n} \Phi_I^\top \Phi_T, C_{TT} = \frac{1}{n} \Phi_T^\top \Phi_T$$

Note that the above matrix is PSD, which implies that we can leverage the Schur complement to decompose the image-based block C_{II} as follows:

$$C_{II} = \underbrace{C_{II} - C_{IT} C_{TT}^{-1} C_{IT}^\top}_{\text{Image component } \Lambda_I} + \underbrace{C_{IT} C_{TT}^{-1} C_{IT}^\top}_{\text{text component } \Lambda_T} \quad (6)$$

Proposition 1. Define text-to-image conversion matrix $\Gamma^* = C_{TI} C_{TT}^{-1}$. Then, Γ^* is an optimal solution to the following ($\|\cdot\|_F$ denotes the Frobenius norm):

$$\operatorname{argmin}_{\Gamma \in \mathbb{R}^{d \times d}} \frac{1}{n} \left\| \Phi_I^\top - \Gamma \Phi_T^\top \right\|_F^2$$

Then, in equation 6, Λ_T is the covariance matrix of $\Gamma^* \phi(x_T)$, and Λ_I is the kernel covariance matrix of $\phi(x_I) - \Gamma^* \phi(x_T)$.

Remark 1. Proposition 1 shows that given the optimal text-to-image conversion matrix $\Gamma^* = C_{TI} C_{TT}^{-1}$, the effect of a text T on the embedding of an image I can be canceled by considering the remainder term $\phi(x_I) - \Gamma^* \phi(x_T)$ to decorrelate the image and text embedding.

Following the above discussion for the cosine-similarity kernel $\phi(x) = x/\|x\|$, we can modify the CLIP embedding given a paired dataset of prompts and images. To do this, we first compute the modification matrix $\Gamma^* = C_{TI}C_{TT}^{-1}$ and modify the CLIP embedding for an image sample $x_I = \text{CLIP}(I)$ and correcting prompt $x_T = \text{CLIP}(T)$ as:

$$\text{CLIP}_{\text{modified}}(I|T) := \text{CLIP}(I) - \Gamma^* \text{CLIP}(T) \quad (7)$$

Note that using the cosine similarity kernel, the dimension of Γ^* matches with the CLIP dimension, i.e., 512.

Furthermore, in the decomposition in equation 6, both the image component Λ_I and the text component Λ_T are PSD matrices, which have non-unit trace values. To apply the matrix-based entropy definition which requires the unit trace, we rewrite the identity as

$$C_{II} = \text{Tr}(\Lambda_I) \cdot \frac{1}{\text{Tr}(\Lambda_I)} \Lambda_I + (1 - \text{Tr}(\Lambda_I)) \cdot \frac{1}{\text{Tr}(\Lambda_T)} \Lambda_T$$

Following the above decomposition, we define the Schur-Complement-Entropy for the image part SCE_I as follows:

$$\text{SCE}_I(x_1, \dots, x_n) := \sum_{j=1}^d \lambda_j^{(\Lambda_I)} \log \frac{\text{Tr}(\Lambda_I)}{\lambda_j^{(\Lambda_I)}} \quad (8)$$

where $\lambda_j^{(\Lambda_I)}$ denotes the j th eigenvalue of matrix Λ_I and $\text{Tr}(\Lambda_I) = \sum_{j=1}^d \lambda_j^{(\Lambda_I)}$ is the sum of the eigenvalues. It can be seen that the defined Schur complement entropy is the conditional entropy of the hidden image cluster variable $\text{Mode} \in \{1, 2, \dots, d\}$, which follows the spectral decomposition of the image covariance matrix $C_{II} = \sum_{j=1}^d \lambda_j v_j v_j^\top$, where the mode $\text{Mode} = i$ has probability λ_i . Here we define a text-based guess of the image mode Y_T , which as we discuss in the Appendix can correctly predict the cluster with probability $\text{Tr}(\Lambda_T)$ and outputs erasure e with probability $\text{Tr}(\Lambda_I)$. Then, we show in the Appendix that following standard Shannon entropy definition:

$$\text{SCE}_I(x_1, \dots, x_n) = H(\text{Mode}|Y_T)$$

Therefore, this analysis allows us to decompose the diversity of generated images into model-driven and text-driven components.

5 Numerical Results

We evaluated our proposed Schur Complement-based approach for CLIP decomposition across various scenarios using both real and synthetic datasets. Our experimental results are reported for the standard Cosine Similarity and Gaussian kernel functions. For the Gaussian kernel function, we use random Fourier features [26] with a random Fourier dimension $r = 2000$ to embed the kernel using a finite feature dimension. In the diversity evaluation, we report our defined SCE scores as well as the Vendi score [6], RKE [18], Recall [4] and Coverage [5] for unconditional diversity assessment without taking the text data into account. Note that Recall and Coverage may only be performed in the presence of a valid representative reference dataset. The clustering experiments were performed using Kernel PCA with the Gaussian kernel, highlighting the top clusters that align with the top eigenvector directions in the data.

Measuring Text-to-Image Model Diversity. To highlight the strengths of SCE-based diversity evaluation, we conducted numerical experiments comparing unconditional and conditional diversity assessments. Figure 3 presents an experiment with the FLUX.1-dev [27] model, where individuals are generated based on an ambiguous prompt. We fixed the text prompt distribution and conditioned the model to generate doctors of varying gender and age. The results show that when the model is restricted to producing only "senior male doctors," the SCE_I score is the lowest. Conversely, when the model generates a broader range of age groups and genders, the diversity score increases. We also provide an interpolated surface plot illustrating the intermediate mixing results. A diversity level of 0 indicates a strong bias toward a single characteristic (e.g., all images depict males), whereas a score of 1 signifies an equal representation of all characteristics (e.g., an equal number of male and female images).

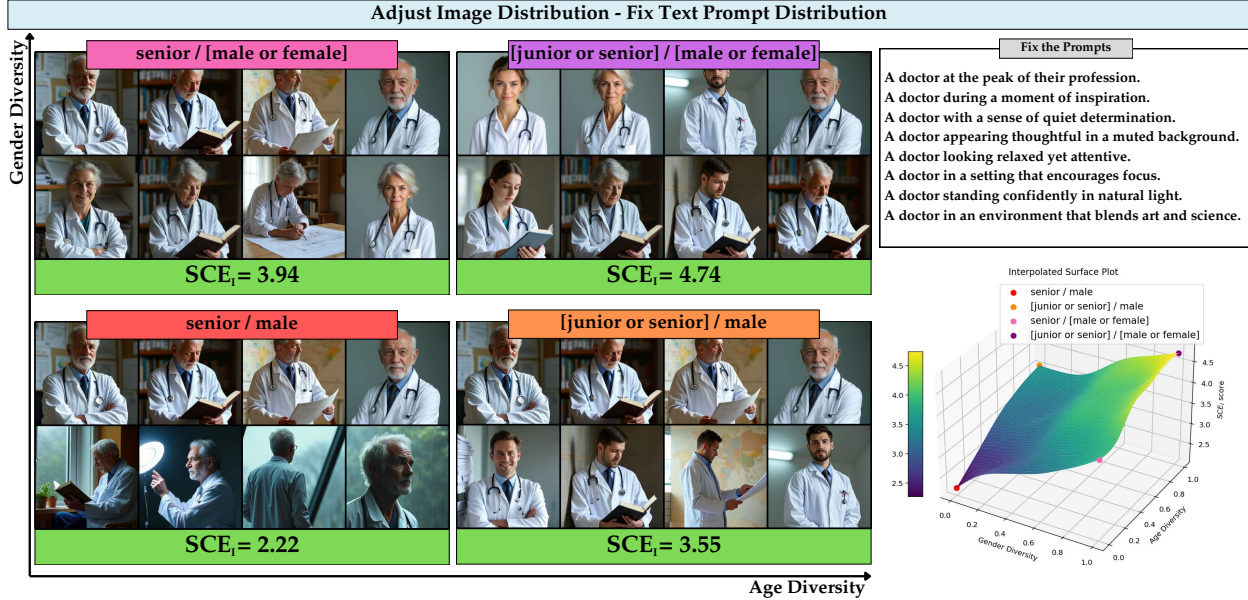


Figure 3: Evaluated SCE_I scores with fixed text prompt distribution about doctors in various settings. Interpolated surface plot in the bottom right visualises the change in diversity (z-axis) when doctors have a varying diversity of age and gender features. (x and y axis)

Figure 4 illustrates the inverse scenario: the image distribution is fixed while the accompanying text prompts vary in their specificity. We generated four sets of "junior male doctor" images with different seeds, while prompts were assigned four levels of detail—fully specified (age and gender), partially specified (age only or gender only), or unspecified (no details). We measured SCE_I , Vendi, RKE, Coverage and Recall scores across four scenarios. Reference set for R/C is "doctor" class in IdenProf dataset [28]. Vendi, RKE, Recall and Coverage scores remain relatively unchanged, whereas SCE_I distinguishes between these cases. When the description is incomplete, SCE_I is lowest due to the strong presence of "junior male doctors" across all images, indicating bias. However, when prompts explicitly state that all images should depict "junior male doctors," diversity increases and is evaluated based on auxiliary features such as background details rather than age or gender. When partial information is given, SCE_I falls between the fully specified and unspecified cases. These results highlight the need for differentiation between model-driven and prompt-driven diversity.

To further quantify our findings, in Figure 5 we conducted an experiment on SDXL generated cat images of different breeds. We generated 1,000 images per class and compared SCE_I with other diversity

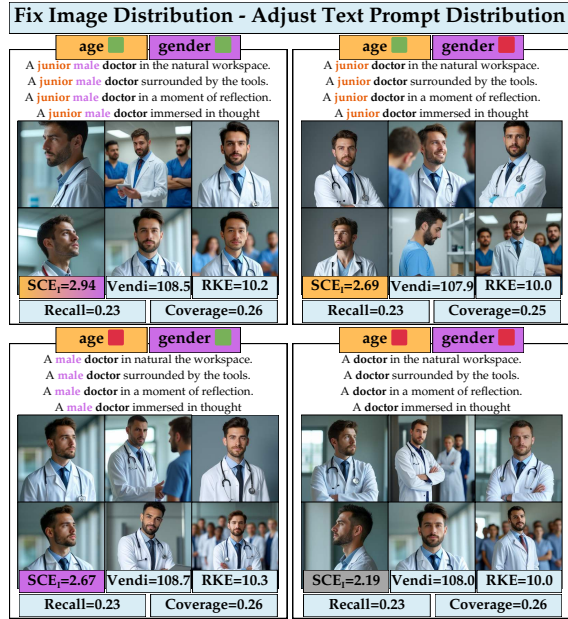


Figure 4: Evaluated SCE_I scores with fixed text prompt distribution. SCE_I changes to reflect the diversity contributed by the varying level of information in text prompts.

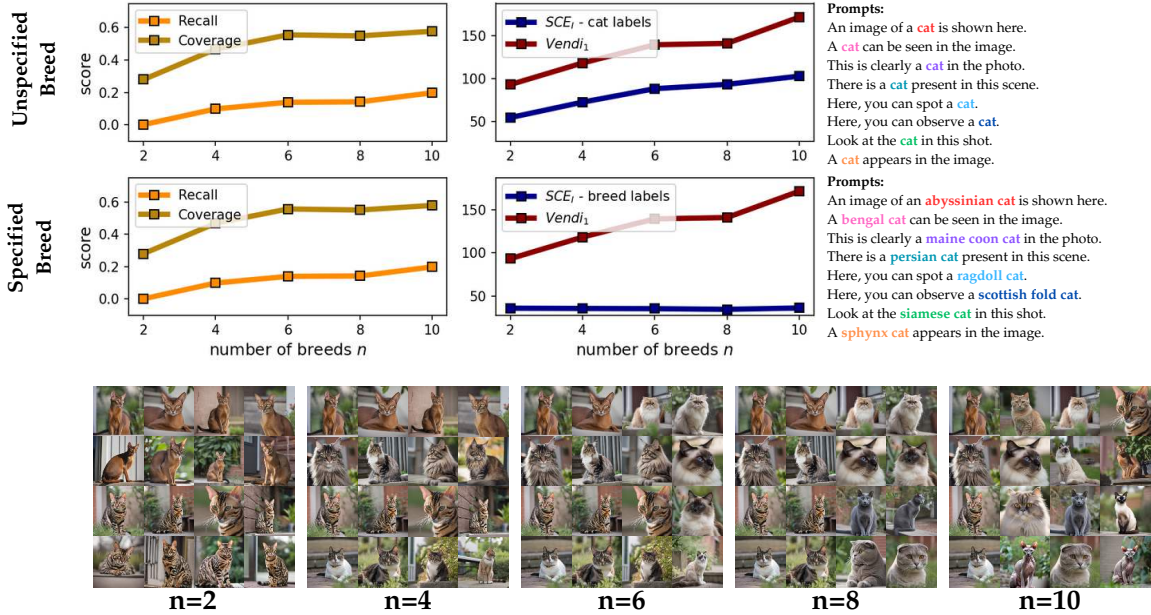


Figure 5: Evaluated SCE_I , Vendi, Recall and Coverage scores with Gaussian Kernel on different cat breeds dataset.

metrics. When prompts did not specify cat breeds, the diversity captured by SCE_I aligns with unconditional Vendi score. Conversely, when breed information was included in the prompts, diversity mainly stemmed from the text prompts rather than the image generator, leading to a non-increasing SCE_I score. In both scenarios, Vendi, Coverage, and Recall scores remained unchanged. The reference set for Recall and Coverage consisted of ImageNet [29] 'cat' samples. Additional experiments on other cases are discussed in the Appendix.

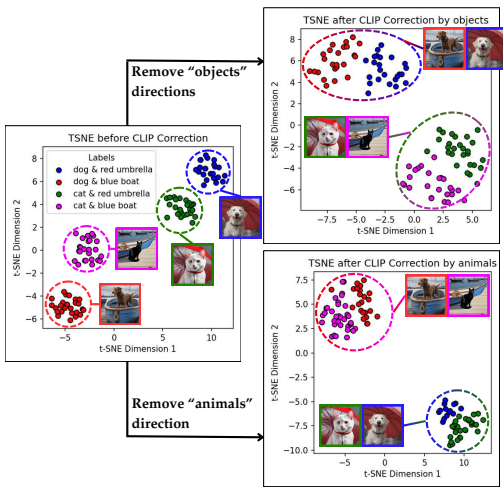
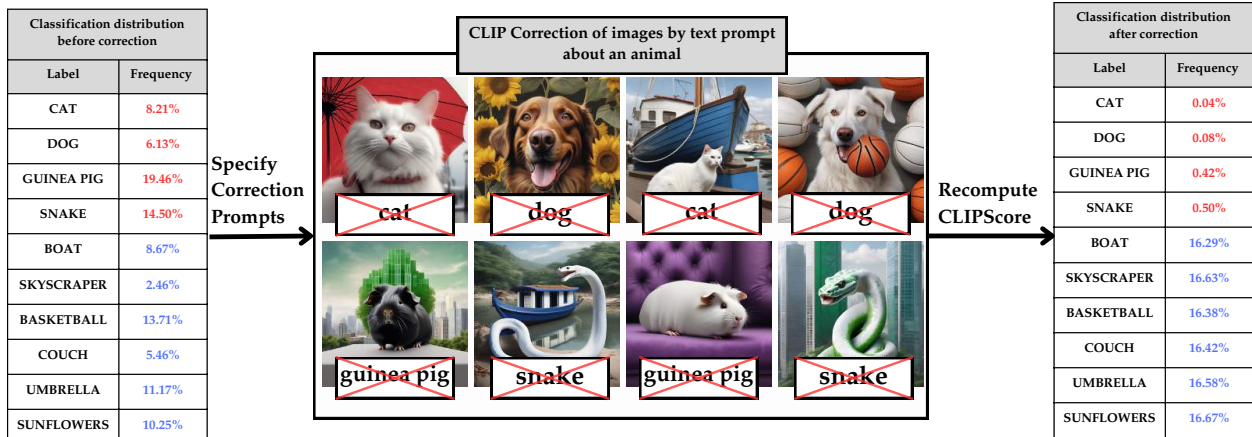


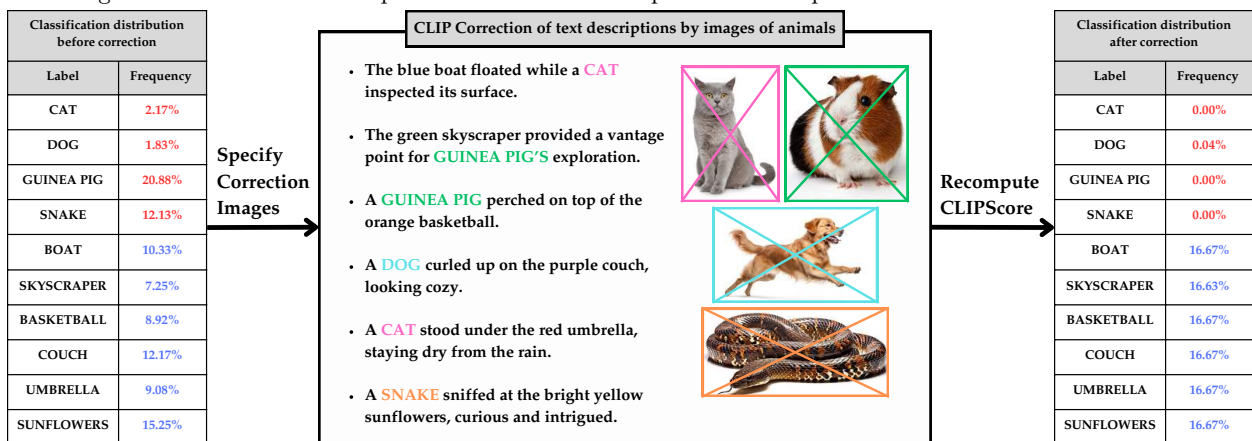
Figure 6: t-SNE plot of animals with objects dataset.

The presented experimental results highlight the importance of disentangling the sources of diversity in text-to-image generation—specifically, the diversity induced by the text prompts versus that originating from the generative model itself. Our findings reveal that when the distribution of prompts or the resulting images is varied, a reliable evaluation metric must be sensitive to both aspects, adapting accordingly to reflect shifts in either distribution. In contrast, existing metrics primarily assess diversity based solely on image features, overlooking the influence of prompt variability. This limitation reduces their effectiveness in scenarios where prompt semantics play a central role, such as in text-to-image generation. These observations motivate the development of a new metric that jointly captures the interplay between prompt diversity and image diversity, enabling more faithful and nuanced evaluation of generative models in this setting.

CLIP Decomposition. To illustrate the effect of Schur-complement-based decomposition on the embedding space, we first generate an "animals with objects" dataset with SDXL, where each sample contains one object from 'boat', 'skyscraper', 'basketball', 'couch', 'umbrella',



(a) Classification distribution before and after CLIP correction on SDXL generated images of animals with objects in the background. The correction is performed via text descriptions of concepts to be removed.



(b) Classification distribution before and after CLIP correction on gpt4o-mini captioned text descriptions about animals with objects in the background. The correction is performed using provided images that encapsulate the concept to be removed.

Figure 7: Classification distribution before and after correction in text-to-image generation and image captioning (image-to-text) tasks

‘sunflowers’ paired with one animal from ‘cat’, ‘dog’, ‘guinea pig’, ‘snake’. In this dataset, diversity increases primarily due to the higher number of subjects rather than feature variations. Using this dataset, we apply t-SNE to visualize the dimensionality-reduced embeddings of CLIP and its corrected variant in Figure 6. The results show that distinct clusters of objects and animals merge when we remove either the "animal" or "object" direction from the embedding, demonstrating the impact of our decomposition. Performing SCE decomposition causes a change in the embedding space and correlation of features along removed direction greatly decreases.

Furthermore, Figure 7 quantifies these effects, showing that CLIP embeddings are initially sensitive to both objects and animals. However, when we specify a prompt to focus on one of these two categories in animal, object and remove its corresponding direction from CLIP, the corrected embedding becomes invariant to that concept. This is evidenced by the second column, where CLIPScore based classification accuracy using the modified embedding significantly drops for the removed component. We highlight that our method is compatible with any embedding as long as it is able to encode both text and image data.

Figure 7b further extends our analysis by applying the SCE-based decomposition not only to the text-to-image setting but also to its inverse: the image-to-text, or image captioning, task. The experimental

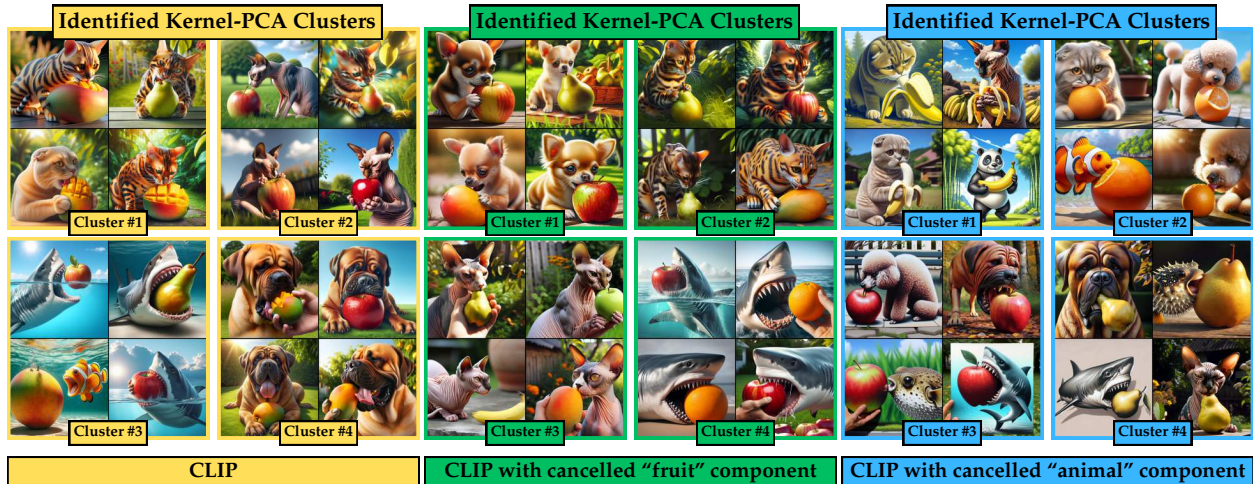


Figure 8: Clusters of DALL-E 3 [7] generated images of animals with fruits. The yellow column shows Kernel-PCA (KPCA) clusters using CLIP; the green column shows KPCA clusters with the application the proposed Schur-Complement-based method to remove "fruit" direction from CLIP embedding; and the blue column shows clusters with the "animal" direction removed from CLIP embedding.

setup mirrors that of Figure 7a, with the key difference being that, instead of generating images for text prompts, we generated captions for the corresponding images. For this task, we used *gpt4o-mini* as the captioning model. We selected images closely aligned with the concept we aimed to remove. For instance, to eliminate the "cat" direction in text, we used an image of a cat against a white background to better isolate the concept. After applying corrections for "animals" or "objects" in the text prompt, we observed successful decomposition, as reflected in the second column: the corrected CLIP embedding is no longer sensitive to the removed concept. The results closely mirror those observed in the text-to-image case, reinforcing that our decomposition method consistently removes the influence of the specified concept across both textual and visual modalities. This symmetry highlights the robustness of our approach in isolating concept-driven variations, regardless of the generation direction. Our method can be readily extended to other paired tasks, provided that an appropriate embedding model exists to encode the paired modalities.

Additionally, we use the eigenspace of the Schur complement component to interpret the diversity in the generated images that is independent of the text prompt, revealing the unique elements introduced by the generation model in the images. The eigenspace-based interpretation follows the application of the Kernel PCA (KPCA) clustering method and leads to a visualization of the sample clusters due to the input text clusters and the clusters with a feature added by the model to the generated image. Figure 8 shows the resulting KPCA-detected clusters for DALL-E 3 [7] generated images in response to prompts of type "[animal] eating a [fruit]" with 5 different animal and fruit names. The detected clusters of CLIP image embedding (leftmost case) shows clusters with mixed animals and fruits. On the other hand, by considering the prompt of only specifying the fruit, the Schur complement component's KPCA clusters highlight the animals in each cluster (middle case), and similarly by considering the prompt of only specifying the animal, the animals are captured by each KPCA cluster of the Schur complement matrix. Further decomposition results and analysis are provided in the Appendix.

Moreover, to test how CLIP correction affects the underlying directions of concepts, we applied CLIPDiffusion [30] framework to edit the image according to different CLIP embeddings. Figure 9 illustrates the setup of the problem, where we edit 'initialization image' that consists of two subjects: a cat and a basketball. Next we denoise and guide the generation according to three different embeddings: Unchanged CLIP embedding of 'initialization image', corrected CLIP by a 'cat' direction or corrected CLIP by a 'basketball' direction. We show that after removing a concept direction, denoiser is no longer rewarded for generating corresponding concept, which is reflected in denoised images. A basketball after correction resembles a bowl with plants and cat loses all of its features. We also note that in both cases, the other object remains intact. To further

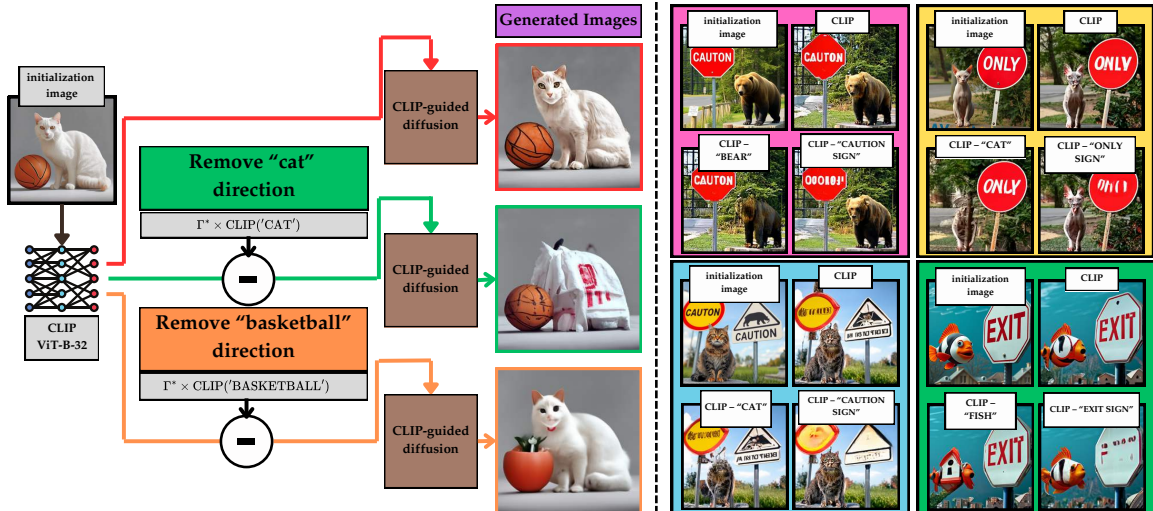


Figure 9: CLIP-guided diffusion process. Starting from an 'initialization image,' generation is guided by CLIP embeddings. The baseline (red arrow) shows unchanged denoising. Adjusted CLIP-guided results (green and orange arrows) show denoised images after removing one of the subjects. Additional clip-guided denoised samples are shown on the right.

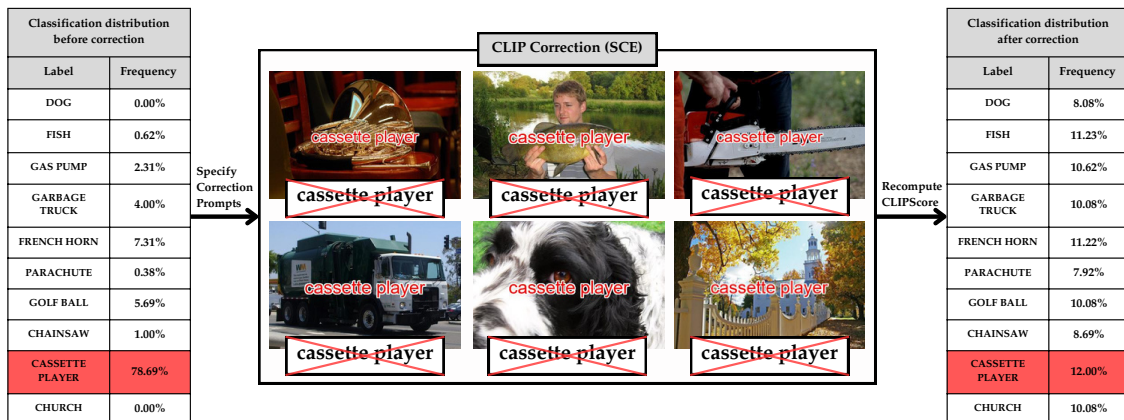


Figure 10: Effect of removing encoded "cassette player" text on top of ImageNet samples.

showcase these results, we performed the same diffusion on the animals with traffic signs dataset shown on the side of Figure 9. This experiment offers a visual interpretation of how the decomposition process removes specific directional components and what the resulting corrected embedding represents. While the SCE-based decomposition is not intended for direct application in image editing tasks, these results are illustrative of the changes that occur in the embedding space when a particular concept is removed from an image. To further validate our approach, we include a baseline where the correction matrix is set to $\Gamma^* = I$, effectively bypassing the optimization step. In this setting, the resulting embeddings fail to preserve the original semantic directions and deviate significantly from the expected outcomes, underscoring the importance of computing the optimal correction matrix Γ^* for meaningful concept removal. The additional results are provided in the Appendix.

Typographic Attacks. CLIP's sensitivity to text within images, as showed in [13], makes it vulnerable to typographic attacks, where overlaying misleading text on an image influences its classification [31]. To investigate this, we constructed a dataset of 10 ImageNet classes, each image engraved with a random class label. We conducted an experiment to evaluate the classification performance of CLIP before and after applying our correction method. Figure 10 presents the distribution of predicted classes for images

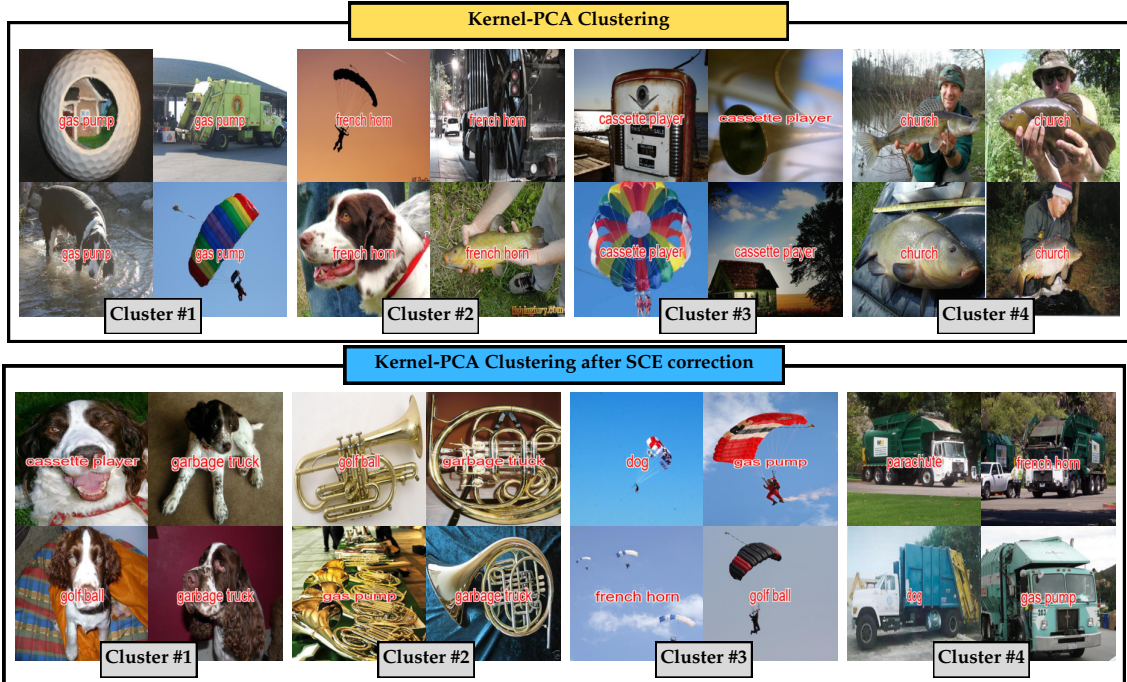


Figure 11: Kernel PCA clusters before and after CLIP correction on captioned ImageNet dataset.

overlaid with the text "cassette player." Prior to correction, CLIP misclassified nearly 79% of these images as "cassette player," indicating a strong susceptibility to typographic bias. However, after applying the SCE-based correction, the misclassification rate drops dramatically to 12%, demonstrating the effectiveness of our approach in mitigating the effect of a typographic attack in the embedding space.

Furthermore, Figure 11 demonstrates CLIP's susceptibility, showing that top eigenvector directions capture the engraved text rather than the actual image content. By conditioning on prompts like "text reading 'cassette player' on top of image" and removing this direction, we re-clustered images based on the corrected CLIP embedding. This adjustment allowed us to identify clusters based on the actual image content rather than the engraved text. We visualize the top modes associated with the leading eigenvectors, revealing that the original CLIP embeddings tend to cluster images based on the overlaid text (e.g., text in the center of the image), rather than the actual image content. In contrast, the SCE-corrected CLIP embeddings cluster images according to their visual content, effectively ignoring the spurious text signal.

6 Conclusion

In this work, we proposed a Schur Complement-based approach to decompose the kernel covariance matrix of CLIP image embeddings into the sum of text-induced and model-induced kernel covariance components. We demonstrated the application of this Schur Complement-based approach for evaluating the diversity of text-to-image models' generated data based on the model's input text. This method extends the application of CLIP embeddings from relevance evaluation to assessing diversity in text-to-image generation models. Additionally, we applied our approach to modify CLIP image embeddings by modifying or canceling the influence of an input text. Our numerical results showcase the potential for canceling text effects and its applications to computer vision tasks. Future research directions include extending the Schur Complement-based approach to other generative AI models, such as text-to-video and language models. Additionally, leveraging this decomposition to fine-tune the CLIP model for enhanced understanding of diverse concepts represents another future direction.

References

- [1] Alec Radford, Jong Wook Kim, Chris Hallacy, Aditya Ramesh, Gabriel Goh, Sandhini Agarwal, Girish Sastry, Amanda Askell, Pamela Mishkin, Jack Clark, Gretchen Krueger, and Ilya Sutskever. Learning transferable visual models from natural language supervision. In Marina Meila and Tong Zhang, editors, *Proceedings of the 38th International Conference on Machine Learning*, volume 139 of *Proceedings of Machine Learning Research*, pages 8748–8763. PMLR, 18–24 Jul 2021.
- [2] Jack Hessel, Ari Holtzman, Maxwell Forbes, Ronan Le Bras, and Yejin Choi. CLIPScore: a reference-free evaluation metric for image captioning. In *EMNLP*, 2021.
- [3] Mehdi SM Sajjadi, Olivier Bachem, Mario Lucic, Olivier Bousquet, and Sylvain Gelly. Assessing generative models via precision and recall. *Advances in neural information processing systems*, 31, 2018.
- [4] Tuomas Kynkäänniemi, Tero Karras, Samuli Laine, Jaakko Lehtinen, and Timo Aila. Improved precision and recall metric for assessing generative models. *Advances in Neural Information Processing Systems*, 32, 2019.
- [5] Muhammad Ferjad Naeem, Seong Joon Oh, Youngjung Uh, Yunjey Choi, and Jaejun Yoo. Reliable fidelity and diversity metrics for generative models. In *International Conference on Machine Learning*, pages 7176–7185. PMLR, 2020.
- [6] Dan Friedman and Adji Bousso Dieng. The vendi score: A diversity evaluation metric for machine learning. *Transactions on machine learning research*, 2023.
- [7] OpenAI. Dall-e 3. <https://openai.com/index/dall-e-3/>. Accessed: 2024-10-30.
- [8] Ramprasaath R. Selvaraju, Michael Cogswell, Abhishek Das, Ramakrishna Vedantam, Devi Parikh, and Dhruv Batra. Grad-cam: Visual explanations from deep networks via gradient-based localization. In *ICCV*, pages 618–626. IEEE Computer Society, 2017.
- [9] Mukund Sundararajan, Ankur Taly, and Qiqi Yan. Axiomatic attribution for deep networks. *CoRR*, abs/1703.01365, 2017.
- [10] Hila Chefer, Shir Gur, and Lior Wolf. Transformer interpretability beyond attention visualization. In *Proceedings of the IEEE/CVF Conference on Computer Vision and Pattern Recognition (CVPR)*, pages 782–791, June 2021.
- [11] Yossi Gandelsman, Alexei A Efros, and Jacob Steinhardt. Interpreting CLIP’s image representation via text-based decomposition. In *The Twelfth International Conference on Learning Representations*, 2024.
- [12] Usha Bhalla, Alex Oesterling, Suraj Srinivas, Flavio P. Calmon, and Himabindu Lakkaraju. Interpreting clip with sparse linear concept embeddings (splice). In *Advances in Neural Information Processing Systems*, 2024.
- [13] Joanna Materzynska, Antonio Torralba, and David Bau. Disentangling visual and written concepts in clip. In *CVPR*, 2022.
- [14] Martin Heusel, Hubert Ramsauer, Thomas Unterthiner, Bernhard Nessler, and Sepp Hochreiter. Gans trained by a two time-scale update rule converge to a local nash equilibrium. *Advances in neural information processing systems*, 30, 2017.
- [15] Miłkołaj Bińkowski, Danica J Sutherland, Michael Arbel, and Arthur Gretton. Demystifying mmd gans. *arXiv preprint arXiv:1801.01401*, 2018.
- [16] Tim Salimans, Ian Goodfellow, Wojciech Zaremba, Vicki Cheung, Alec Radford, Xi Chen, and Xi Chen. Improved techniques for training GANs. In D. Lee, M. Sugiyama, U. Luxburg, I. Guyon, and R. Garnett, editors, *Advances in Neural Information Processing Systems*, volume 29. Curran Associates, Inc., 2016.

- [17] Amey Pasarkar and Adji Bousso Dieng. Cousins of the vendi score: A family of similarity-based diversity metrics for science and machine learning. In *International Conference on Artificial Intelligence and Statistics*. PMLR, 2024.
- [18] Mohammad Jalali, Cheuk Ting Li, and Farzan Farnia. An information-theoretic evaluation of generative models in learning multi-modal distributions. In *Thirty-seventh Conference on Neural Information Processing Systems*, 2023.
- [19] Azim Ospanov, Jingwei Zhang, Mohammad Jalali, Xuenan Cao, Andrej Bogdanov, and Farzan Farnia. Towards a scalable reference-free evaluation of generative models. In *The Thirty-eighth Annual Conference on Neural Information Processing Systems*, 2024.
- [20] Dongkyun Kim, Mingi Kwon, and Youngjung Uh. Attribute based interpretable evaluation metrics for generative models. In *Forty-first International Conference on Machine Learning*, 2024.
- [21] Terrance DeVries, Adriana Romero, Luis Pineda, Graham W. Taylor, and Michal Drozdal. On the evaluation of conditional gans, 2019.
- [22] Tony Lee, Michihiro Yasunaga, Chenlin Meng, Yifan Mai, Joon Sung Park, Agrim Gupta, Yunzhi Zhang, Deepak Narayanan, Hannah Benita Teufel, Marco Bellagente, Minguk Kang, Taesung Park, Jure Leskovec, Jun-Yan Zhu, Li Fei-Fei, Jiajun Wu, Stefano Ermon, and Percy Liang. Holistic evaluation of text-to-image models. In *Thirty-seventh Conference on Neural Information Processing Systems Datasets and Benchmarks Track*, 2023.
- [23] Percy Liang, Rishi Bommasani, Tony Lee, Dimitris Tsipras, Dilara Soylu, Michihiro Yasunaga, Yian Zhang, Deepak Narayanan, Yuhuai Wu, Ananya Kumar, Benjamin Newman, Binhang Yuan, Bobby Yan, Ce Zhang, Christian Alexander Cosgrove, Christopher D Manning, Christopher Re, Diana Acosta-Navas, Drew Arad Hudson, Eric Zelikman, Esin Durmus, Faisal Ladhak, Frieda Rong, Hongyu Ren, Huaxiu Yao, Jue WANG, Keshav Santhanam, Laurel Orr, Lucia Zheng, Mert Yuksekgonul, Mirac Suzgun, Nathan Kim, Neel Guha, Niladri S. Chatterji, Omar Khattab, Peter Henderson, Qian Huang, Ryan Andrew Chi, Sang Michael Xie, Shibani Santurkar, Surya Ganguli, Tatsunori Hashimoto, Thomas Icard, Tianyi Zhang, Vishrav Chaudhary, William Wang, Xuechen Li, Yifan Mai, Yuhui Zhang, and Yuta Koreeda. Holistic evaluation of language models. *Transactions on Machine Learning Research*, 2023. Featured Certification, Expert Certification.
- [24] Pietro Astolfi, Marlene Careil, Melissa Hall, Oscar Mañas, Matthew Muckley, Jakob Verbeek, Adriana Romero Soriano, and Michal Drozdal. Consistency-diversity-realism pareto fronts of conditional image generative models, 2024.
- [25] Nithish Kannan, Arif Ahmad, Marco Andreetto, Vinodkumar Prabhakaran, Utsav Prabhu, Adji Bousso Dieng, Pushpak Bhattacharyya, and Shachi Dave. Beyond aesthetics: Cultural competence in text-to-image models, 2024.
- [26] Ali Rahimi and Benjamin Recht. Random features for large-scale kernel machines. *Advances in neural information processing systems*, 20, 2007.
- [27] Black Forest Lab. Flux: A diffusion-based text-to-image (t2i) model. <https://github.com/blackforestlab/flux>, 2024. Accessed: 2024-09.
- [28] Olafenwa Moses. Idenprof: A pre-trained deep learning model for identifying professionals in images, 2018. Accessed: 2025-03-08.
- [29] Jia Deng, Wei Dong, Richard Socher, Li-Jia Li, Kai Li, and Li Fei-Fei. Imagenet: A large-scale hierarchical image database. In *2009 IEEE conference on computer vision and pattern recognition*, pages 248–255. Ieee, 2009.

- [30] Gwanghyun Kim, Taesung Kwon, and Jong Chul Ye. Diffusionclip: Text-guided diffusion models for robust image manipulation. In *Proceedings of the IEEE/CVF Conference on Computer Vision and Pattern Recognition (CVPR)*, pages 2426–2435, June 2022.
- [31] Yoann Lemesle, Masataka Sawayama, Guillermo Valle-Perez, Maxime Adolphe, H el ene Sauz eon, and Pierre-Yves Oudeyer. Language-biased image classification: evaluation based on semantic representations. In *International Conference on Learning Representations*, 2022.
- [32] Aditya Ramesh, Prafulla Dhariwal, Alex Nichol, Casey Chu, and Mark Chen. Hierarchical text-conditional image generation with clip latents, 2022.
- [33] Anton Razzhigaev, Arseniy Shakhmatov, Anastasia Maltseva, Vladimir Arkhipkin, Igor Pavlov, Ilya Ryabov, Angelina Kuts, Alexander Panchenko, Andrey Kuznetsov, and Denis Dimitrov. Kandinsky: an improved text-to-image synthesis with image prior and latent diffusion, 2023.
- [34] Tsung-Yi Lin, Michael Maire, Serge Belongie, Lubomir Bourdev, Ross Girshick, James Hays, Pietro Perona, Deva Ramanan, C. Lawrence Zitnick, and Piotr Doll ar. Microsoft coco: Common objects in context, 2015.

A Proofs

A.1 Proof of Proposition 1

We aim to solve the optimization problem:

$$\Gamma^* = \underset{\Gamma \in \mathbb{R}^{d \times d}}{\operatorname{argmin}}; \frac{1}{n} \|\Phi_I^\top - \Gamma \Phi_T^\top\|_F^2,$$

where $\Phi_I, \Phi_T \in \mathbb{R}^{d \times n}$ are given matrices, and $\|\cdot\|_F$ denotes the Frobenius norm.

To find the optimal Γ^* , we begin by expanding the objective function. Recall that the squared Frobenius norm of a matrix A is given by $\|A\|_F^2 = \operatorname{Tr}(A^\top A)$. Therefore, we have:

$$\begin{aligned} f(\Gamma) &= \frac{1}{n} \|\Phi_I^\top - \Gamma \Phi_T^\top\|_F^2 \\ &= \frac{1}{n} \operatorname{Tr} \left[(\Phi_I^\top - \Gamma \Phi_T^\top)^\top (\Phi_I^\top - \Gamma \Phi_T^\top) \right] \\ &= \frac{1}{n} \operatorname{Tr} \left[\Phi_I \Phi_I^\top - \Gamma \Phi_I \Phi_T^\top - \Phi_T \Phi_I^\top \Gamma^\top + \Gamma \Phi_T \Phi_T^\top \Gamma^\top \right]. \end{aligned}$$

Let us define the covariance matrices:

$$\begin{aligned} C_{II} &= \Phi_I \Phi_I^\top \in \mathbb{R}^{d \times d}, \\ C_{IT} &= \Phi_I \Phi_T^\top \in \mathbb{R}^{d \times d}, \\ C_{TI} &= \Phi_T \Phi_I^\top = C_{IT}^\top \in \mathbb{R}^{d \times d}, \\ C_{TT} &= \Phi_T \Phi_T^\top \in \mathbb{R}^{d \times d}. \end{aligned}$$

Substituting these definitions into $f(\Gamma)$, we obtain:

$$f(\Gamma) = \frac{1}{n} \operatorname{Tr} \left[C_{II} - \Gamma C_{IT} - C_{TI} \Gamma^\top + \Gamma C_{TT} \Gamma^\top \right].$$

To find the minimizer, we compute the Jacobian of $f(\Gamma)$ with respect to Γ . Using standard matrix derivative identities, we have:

$$\begin{aligned} \mathbf{J}_\Gamma f(\Gamma) &= \frac{1}{n} (-C_{IT}^\top - C_{TI} + 2\Gamma C_{TT}) \\ &= \frac{1}{n} (-C_{IT}^\top - C_{IT}^\top + 2\Gamma C_{TT}) \quad (\text{since } C_{TI} = C_{IT}^\top) \\ &= \frac{1}{n} (-2C_{IT}^\top + 2\Gamma C_{TT}). \end{aligned}$$

We observe that by choosing $\Gamma^* = C_{TI} C_{TT}^{-1}$, we will have

$$\mathbf{J}_\Gamma f(\Gamma^*) = -\frac{2}{n} C_{IT}^\top + \frac{2}{n} \Gamma^* C_{TT} = \mathbf{0}.$$

Therefore, Γ^* is a stationary point in the optimization problem with a convex objective function and hence is an optimal solution to the minimization task.

A.2 Conditional Entropy Interpretation of SCE Score

As discussed in the main text, in Equation equation 6, both image component Λ_I and text component Λ_T are PSD matrices with unit trace. Furthermore, we have

$$C_{II} = \operatorname{Tr}(\Lambda_I) \cdot \frac{1}{\operatorname{Tr}(\Lambda_I)} \Lambda_I + (1 - \operatorname{Tr}(\Lambda_I)) \cdot \frac{1}{\operatorname{Tr}(\Lambda_T)} \Lambda_T$$

Next, we consider the spectral decomposition of matrix $C_{II} = \sum_{i=1}^d \lambda_i \mathbf{v}_i \mathbf{v}_i^\top$ given its non-negative eigenvalues $\lambda_1 \geq \dots \geq \lambda_d$ and orthonormal eigenvectors $\mathbf{v}_1, \dots, \mathbf{v}_n$. Following the orthonormality of the eigenvectors, we have the following for every $j \in \{1, \dots, d\}$:

$$\lambda_j = \text{Tr}(\Lambda_I) \cdot \frac{1}{\text{Tr}(\Lambda_I)} \mathbf{v}_j^\top \Lambda_I \mathbf{v}_j + (1 - \text{Tr}(\Lambda_I)) \cdot \frac{1}{\text{Tr}(\Lambda_T)} \mathbf{v}_j^\top \Lambda_T \mathbf{v}_j$$

Therefore, if we define the Mode random variable over $\{1, \dots, d\}$ with probabilities $\lambda_1, \dots, \lambda_d$, its unconditional Shannon entropy will be $H(\text{Mode}) = \sum_{i=1}^d \lambda_i \log(1/\lambda_i)$. On the other hand, if an adversary has the side knowledge of the text it can correctly predict $\text{Mode} = j$ with probability $\mathbf{v}_j^\top \Lambda_T \mathbf{v}_j$. If we define Y_{adv} as the correct prediction of this adversary when the text can be correctly mapped to the mode variable and else we define $Y_{\text{adv}} = e$ as the error, then the conditional entropy will be:

$$\begin{aligned} H(\text{Mode}|Y_{\text{adv}}) &= P(Y_{\text{adv}} = e)H(\text{Mode}|Y_{\text{adv}} = e) + P(Y_{\text{adv}} \neq e)H(\text{Mode}|Y_{\text{adv}} \neq e) \\ &= P(Y_{\text{adv}} = e)H(\text{Mode}|Y_{\text{adv}} = e) + P(Y_{\text{adv}} \neq e) \times 0 \\ &= P(Y_{\text{adv}} = e)H(\text{Mode}|Y_{\text{adv}} = e) \\ &= \left(\sum_{j=1}^d \mathbf{v}_j^\top \Lambda_I \mathbf{v}_j \right) \sum_{j=1}^d \frac{\mathbf{v}_j^\top \Lambda_I \mathbf{v}_j}{\sum_{t=1}^d \mathbf{v}_t^\top \Lambda_I \mathbf{v}_t} \log \frac{\sum_{t=1}^d \mathbf{v}_t^\top \Lambda_I \mathbf{v}_t}{\mathbf{v}_j^\top \Lambda_I \mathbf{v}_j} \\ &= \sum_{j=1}^d (\mathbf{v}_j^\top \Lambda_I \mathbf{v}_j) \log \frac{\sum_{t=1}^d \mathbf{v}_t^\top \Lambda_I \mathbf{v}_t}{\mathbf{v}_j^\top \Lambda_I \mathbf{v}_j} \end{aligned}$$

Note that $\sum_{t=1}^d \mathbf{v}_t^\top \Lambda_I \mathbf{v}_t = \sum_{t=1}^d \text{Tr}(\mathbf{v}_t^\top \Lambda_I \mathbf{v}_t) = \text{Tr}(\sum_{t=1}^d \mathbf{v}_t \mathbf{v}_t^\top \Lambda_I) = \text{Tr}(\Lambda_I)$ which implies that

$$\begin{aligned} H(\text{Mode}|Y_{\text{adv}}) &= \sum_{j=1}^d (\mathbf{v}_j^\top \Lambda_I \mathbf{v}_j) \log \frac{\text{Tr}(\Lambda_I)}{\mathbf{v}_j^\top \Lambda_I \mathbf{v}_j} \\ &= \log(\text{Tr}(\Lambda_I)) \left(\sum_{j=1}^d (\mathbf{v}_j^\top \Lambda_I \mathbf{v}_j) \right) + \sum_{j=1}^d (\mathbf{v}_j^\top \Lambda_I \mathbf{v}_j) \log \frac{1}{\mathbf{v}_j^\top \Lambda_I \mathbf{v}_j} \\ &= \log(\text{Tr}(\Lambda_I)) \text{Tr}(\Lambda_I) + \sum_{j=1}^d (\mathbf{v}_j^\top \Lambda_I \mathbf{v}_j) \log \frac{1}{\mathbf{v}_j^\top \Lambda_I \mathbf{v}_j} \end{aligned}$$

which assuming that Λ_I and C_{II} share the same eigenvectors will provide

$$\begin{aligned} H(\text{Mode}|Y_{\text{adv}}) &= \log(\text{Tr}(\Lambda_I)) \text{Tr}(\Lambda_I) + \sum_{j=1}^d (\lambda_j^{(\Lambda_I)}) \log \frac{1}{\lambda_j^{(\Lambda_I)}} \\ &= \sum_{j=1}^d \lambda_j^{(\Lambda_I)} \log \frac{\text{Tr}(\Lambda_I)}{\lambda_j^{(\Lambda_I)}} \end{aligned}$$

Note that the above provides our definition of the Schur-Complement-Entropy for the image part SCE_I and the text part SCE_T as follows:

$$\text{SCE}_I(x_1, \dots, x_n) = \sum_{j=1}^d \lambda_j^{(\Lambda_I)} \log \frac{\text{Tr}(\Lambda_I)}{\lambda_j^{(\Lambda_I)}} \quad (9)$$

$$\text{SCE}_T(x_1, \dots, x_n) := \sum_{j=1}^d \lambda_j^{(\Lambda_T)} \log \frac{\text{Tr}(\Lambda_T)}{\lambda_j^{(\Lambda_T)}} \quad (10)$$

where $\lambda_j^{(\Lambda_I)}$ denotes the j th eigenvalue of matrix Λ_I and $\text{Tr}(\Lambda_I) = \sum_{j=1}^d \lambda_j^{(\Lambda_I)}$ is the sum of the eigenvalues. Note that we follow the same definition for the text part Λ_T .

B Additional Individual Image Decomposition Results via SC-Based Method

In this section, we present additional CLIP decomposition results for randomly selected pairs of ImageNet labels. The correction matrix was computed using the captioned MSCOCO dataset. The experimental setup follows the approach illustrated in Figure 1. We generated images containing predominantly two concepts and applied the SC-based method for decomposition. Subsequently, we measured the cosine similarity between the corrected and regular CLIP embeddings and the CLIP-embedded ImageNet samples. The top four images with the highest similarity scores are reported. These results demonstrate the effectiveness of the Schur Complement method in decomposing directions present in generated images.

Results for synthetic images generated using SDXL are shown in Figures 12 and 13. Corresponding results for DALL-E 3 are presented in Figures 14 and 15. Notably, the Schur Complement-based decomposition successfully isolates and removes image directions corresponding to a text condition that describes the concept to be excluded.

To expand on the results in Figure 8, we constructed a dataset of animals with traffic signs using FLUX.1-schnell [27]. Figure 20 illustrates that after canceling either of the subjects using the Schur complement method, Kernel-PCA clusters according to the remaining concepts in the image.

Moreover, to test how CLIP correction affects the underlying directions of concepts, we applied the CLIPDiffusion [30] framework to edit the image according to different CLIP embeddings. Figure 9 illustrates the setup of the problem, where we edit the 'initialization image' that consists of two subjects: a cat and a basketball. We then denoise and guide the generation according to three different embeddings: the unchanged CLIP embedding of the 'initialization image', the modified CLIP by a 'cat' direction, or the modified CLIP by a 'basketball' direction. We show that after removing a concept direction, the denoiser is no longer rewarded for generating the corresponding concept, which is reflected in the denoised images. After correction, the basketball resembles a bowl with plants, and the cat loses its features. We also note that in both cases, the other object remains intact. To further showcase these results, we performed the same diffusion on the animals with traffic signs dataset, shown on the side of Figure 9.

C Additional Results on Diversity Evaluation

To further validate the findings presented in the main text, we conducted a similar experiment (Figure 5) using the Cosine Similarity Kernel. The results confirm that the diversity trends observed in the main text persist under a finite-dimensional kernel. Figures 16 and 17 illustrate the variation in SCE diversity when conditioned on different text prompts.

Similar to Figure 5, we conducted similar experiment with animals and objects dataset in Figure 18. Our results mirror previous findings, strengthening the proposed diversity evaluation metric in measuring subject quantity related diversity.

Moreover, we evaluate the diversity of typographically attacked ImageNet samples in Figure 21. Specifically, we overlay the text "cassette player" onto images from 10 different ImageNet classes and measure diversity as the number of distinct classes increases. The presence of overlaid text diverts CLIP's sensitivity away from image content, causing it to encode the direction indicated by the text instead.

To illustrate this effect, we visualize salience maps of CLIP embeddings given a prompt referring to an object behind the overlaid text. The results show that CLIP is highly sensitive to centrally placed text, even when it is unrelated to the prompted object. However, applying SC-based decomposition mitigates this bias. This correction is reflected in the diversity plots, where SCE_I increases rapidly as the number of ImageNet classes grows, whereas Vendi, Coverage, and Recall exhibit much weaker correlations with class diversity.

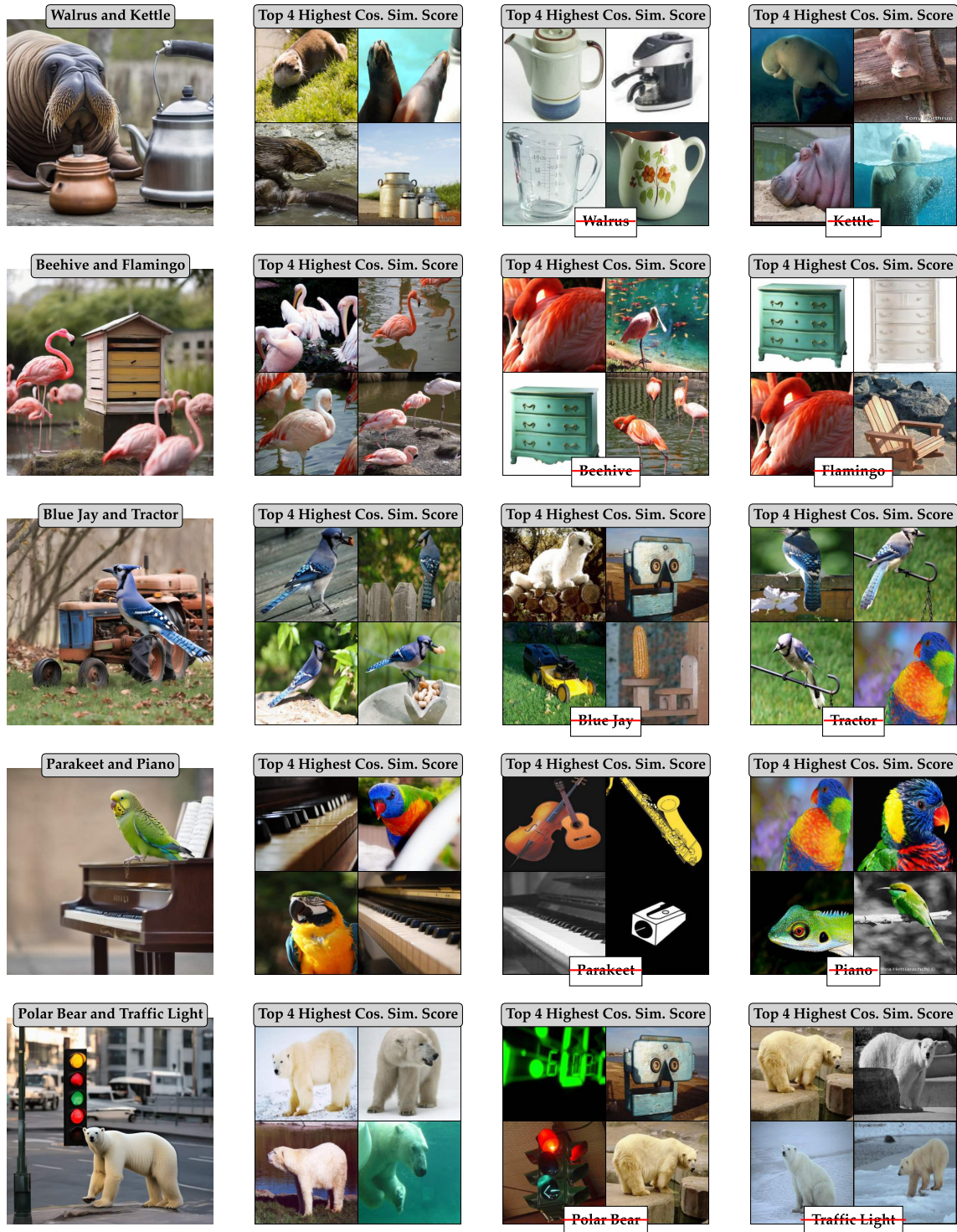


Figure 12: Diagram presenting the decomposition of SDXL generated images of two random labels from ImageNet. First column presents the generated image of a pair. Second column presents four images from ImageNet with highest Cosine Similarity Score. Third and Fourth columns showcase feature removal from the image.

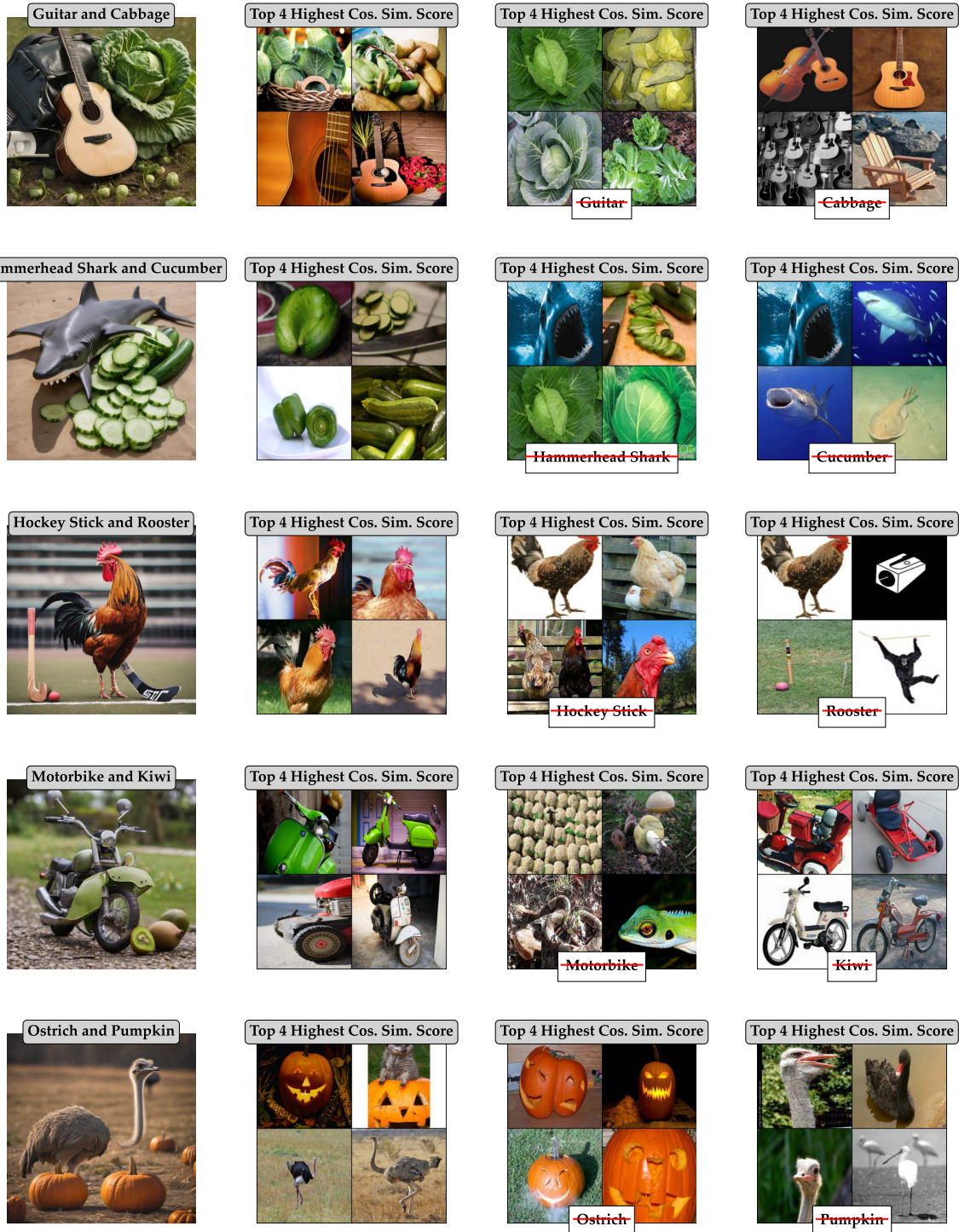


Figure 13: Diagram presenting the decomposition of SDXL generated images of two random labels from ImageNet. First column presents the generated image of a pair. Second column presents four images from ImageNet with highest Cosine Similarity Score. Third and Fourth columns showcase feature removal from the image.

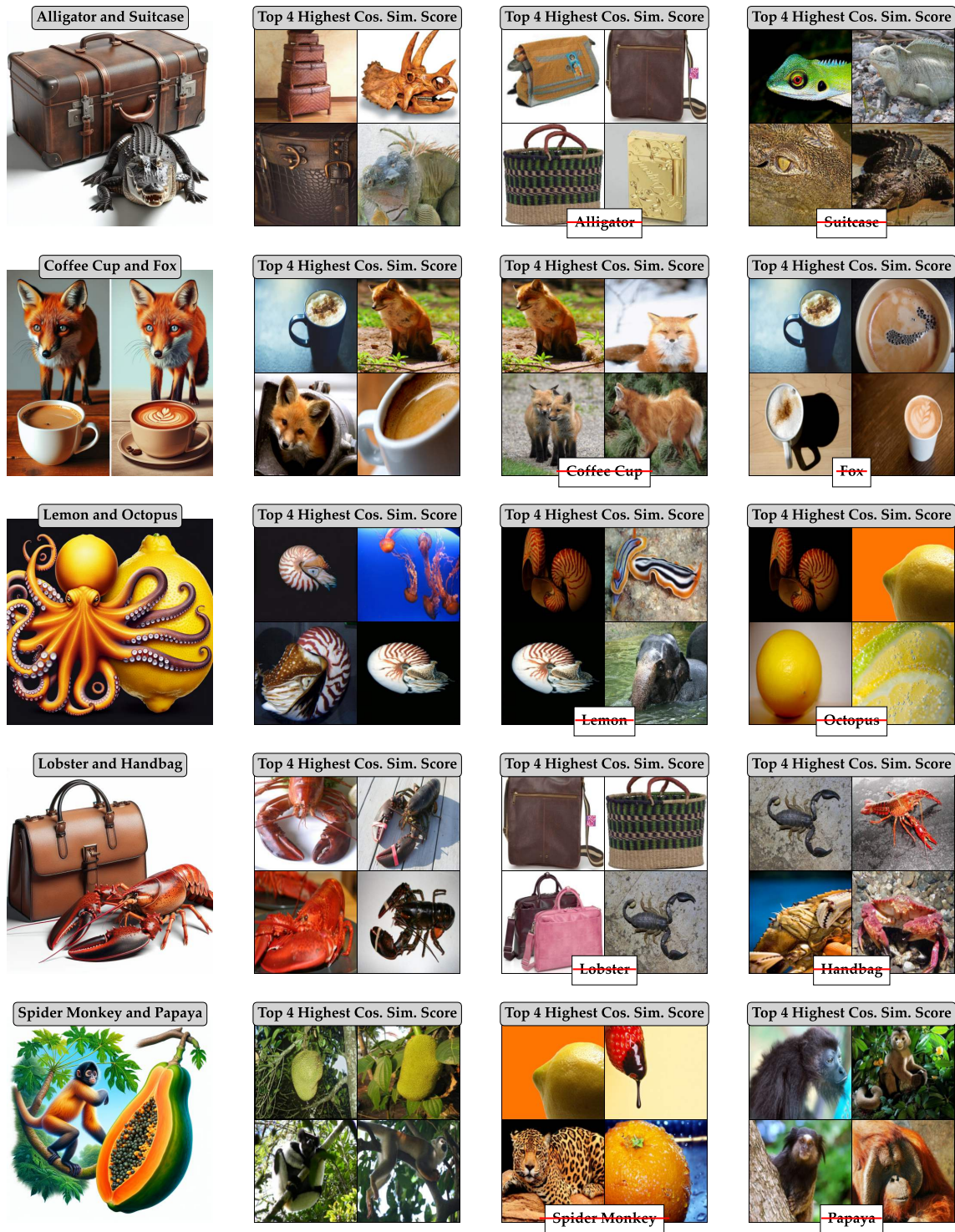


Figure 14: Diagram presenting the decomposition of DALL-E 3 generated images of two random labels from ImageNet. First column presents the generated image of a pair. Second column presents four images from ImageNet with highest Cosine Similarity Score. Third and Fourth columns showcase feature removal from the image.

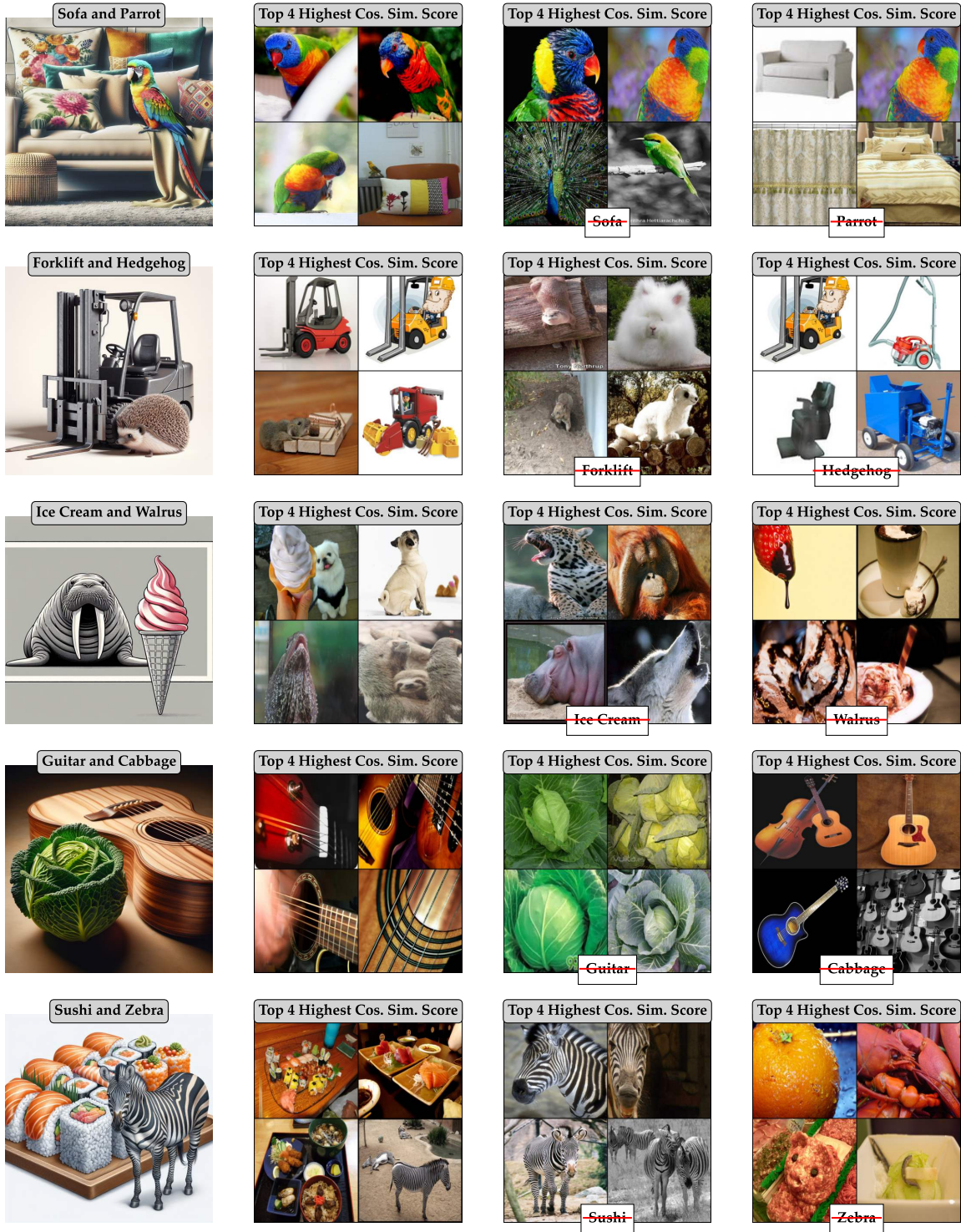


Figure 15: Diagram presenting the decomposition of DALL-E 3 generated images of two random labels from ImageNet. First column presents the generated image of a pair. Second column presents four images from ImageNet with highest Cosine Similarity Score. Third and Fourth columns showcase feature removal from the image.

Cosine Similarity Kernel

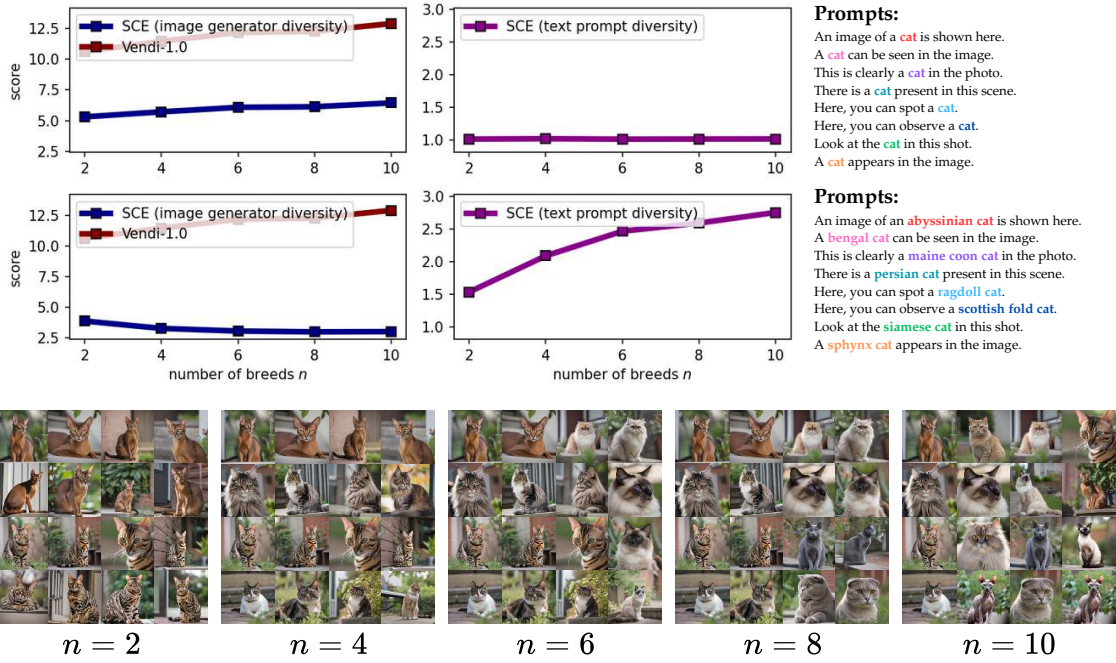


Figure 16: Plots by cancelling out 'cat' and specific cat breed prompts (Cosine Sim Kernel)

Cosine Similarity Kernel

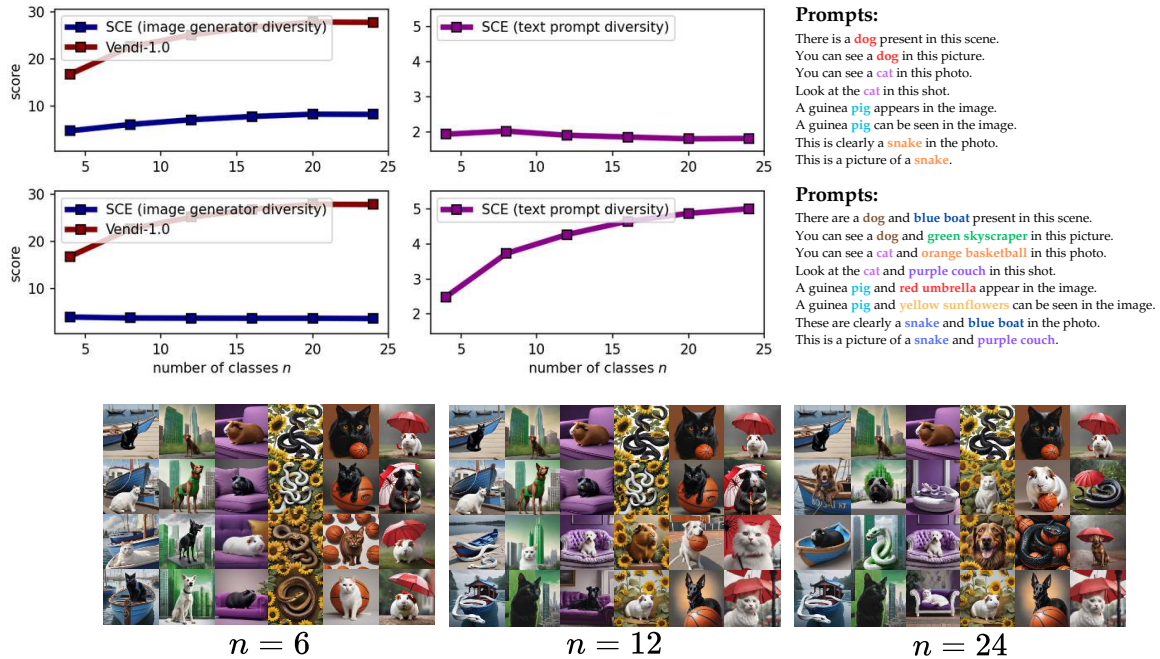


Figure 17: Plots by cancelling out animal name and specific object types prompts (Cosine Sim Kernel)

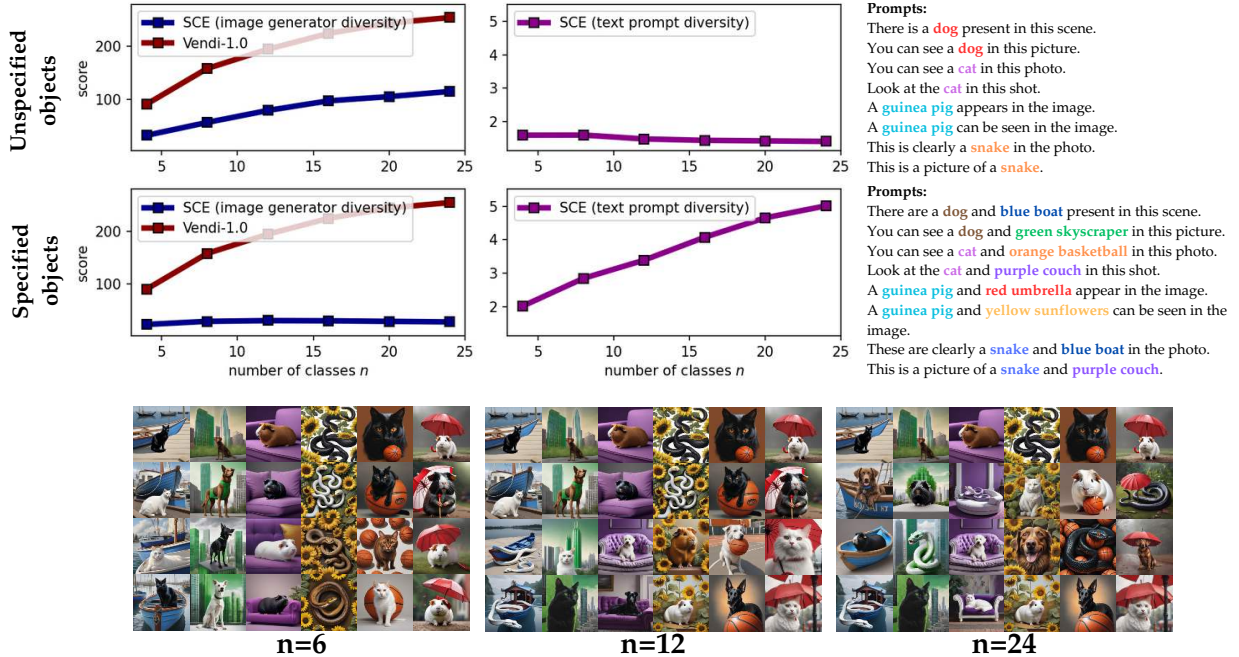


Figure 18: Evaluated SCE and Vendi scores with Gaussian Kernel on different animals with objects.

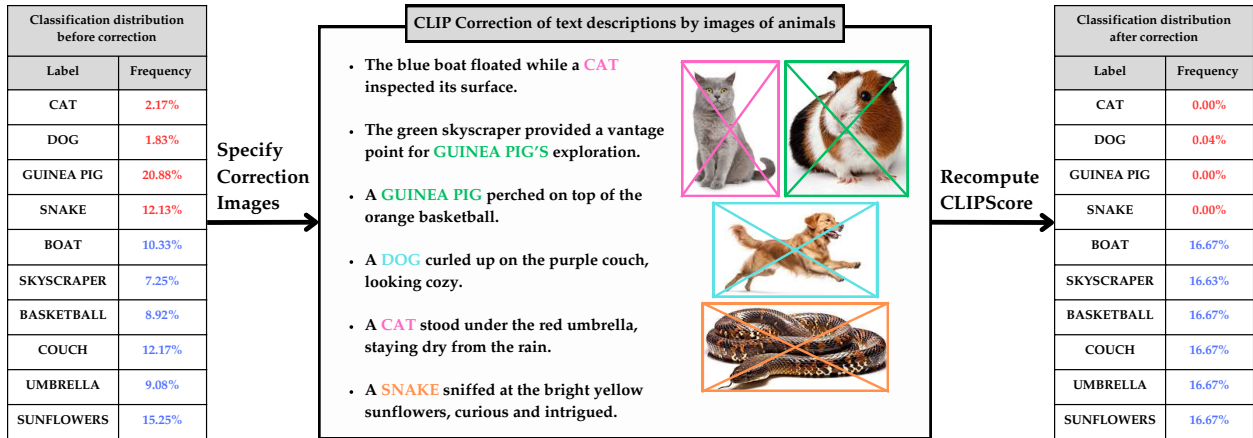
D Results with Naive Text Embedding Subtraction without considering the adjust matrix Γ^*

In the given task setting, it may seem intuitive to assume that the difference between Φ_I and Φ_T would yield a similar outcome as the SC-based decomposition. To test this hypothesis, we compared the SC-based decomposition with a "naive" method, defined as $\Phi_I - \Phi_T$. In this naive approach, the learned correction matrix Γ^* is replaced with an identity matrix, effectively omitting its computation. Our experiments reveal that such a decomposition usually fails to achieve the desired results and often leads to a loss of coherent directionality in the embedding space.

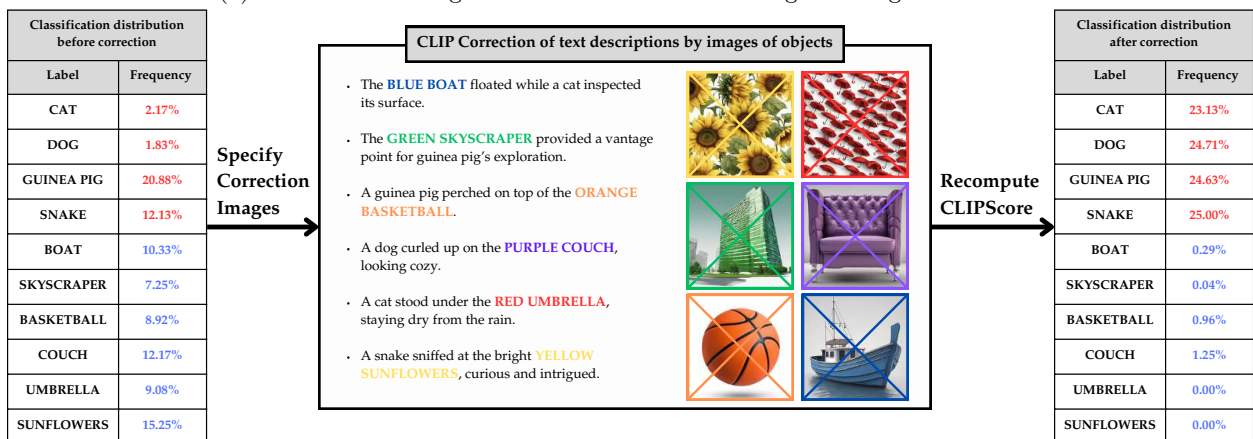
To evaluate the performance of the naive embedding subtraction method, we used the typographic attack dataset, which consists of 10 ImageNet classes where misleading text is overlaid on the images. We measured classification accuracy before and after decomposition. Figure 23 shows the distribution of classifications for images engraved with the text "cassette player." CLIP's classification is heavily biased towards "cassette player," despite the underlying images belonging to a different class. After decomposition, the naive method removes the direction corresponding to the text but results in a skew towards "french horn," even though the image distribution is uniform across all 10 classes. In contrast, the SC-based decomposition corrects the embeddings, making them sensitive to the underlying images rather than the engraved text.

To further demonstrate the effectiveness of the SC method, we compared kernel PCA clusters in Figure 25. The clustering results for the naive decomposition closely resemble those without any correction, indicating that this method does not address the typographic attack. On the other hand, SC-based decomposition significantly improves the clustering by accurately resolving the misleading text directionality.

Additionally, we performed CLIP-guided diffusion to visualize the contents of the corrected embeddings. The setup is illustrated in figure 22 and it is similar to the one described in the main text, except we do not use Γ^* in the decomposition of CLIP. Figure 24 compares images generated using naive and SC-based decompositions. The naive method performs poorly, particularly when text overlays traffic signs, and often removes directions without preserving information about other underlying concepts in the images. In contrast,



(a) Effect of cancelling 'animals' direction from text given images of animals



(b) Effect of cancelling 'objects' direction from text given images of objects

Figure 19: Evaluating the CLIPScore on GPT-4o generated captions of animals with objects

the SC-based decomposition preserves the structural and semantic information while successfully removing the undesired text directionality.

These results highlight the necessity of computing the correction matrix Γ^* to effectively remove specific directions while preserving information about other concepts within the image embeddings.

E Additional Numerical Results

We evaluated several text-to-image models using the SCE metric to assess their performance. Figure 26 summarizes our findings for DALL-E 2 [32], DALL-E 3 [7], Kandinsky 3 [33], and FLUX.1-schnell [27], tested on 5,000 MSCOCO [34] captions.

Our results demonstrate that the SC-Vendi metric correlates with the Vendi score, which measures the diversity of image generators. This suggests that when tested on the MSCOCO dataset, image diversity arises not only from the text prompts but also from the intrinsic properties of the generator itself.

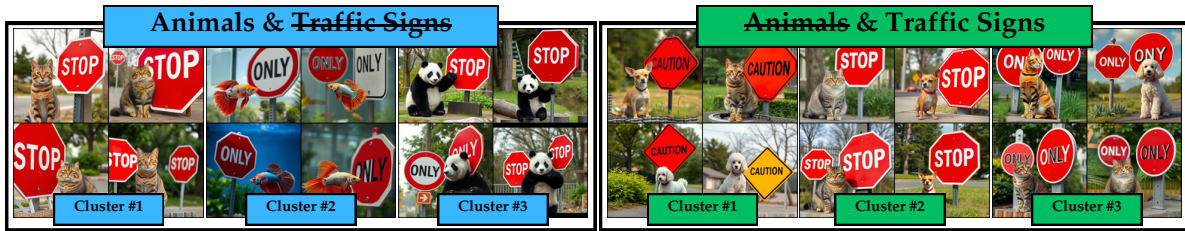


Figure 20: Identified Kernel PCA clusters on the synthetic dataset composed of random animals with traffic signs.

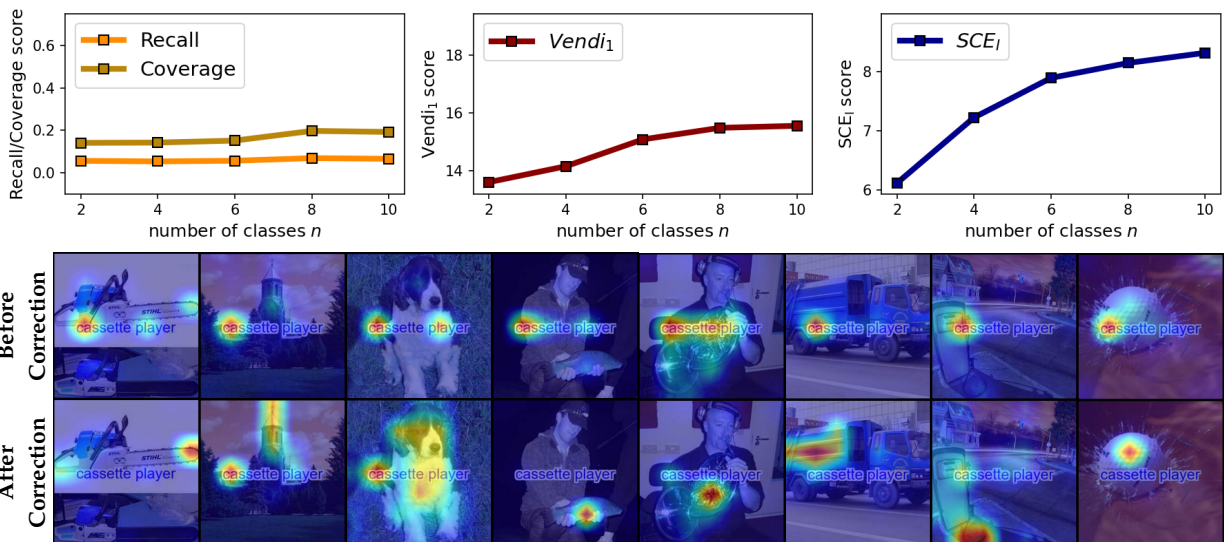


Figure 21: Evaluated SCE, Vendi, Recall and Coverage scores with Gaussian Kernel on ImageNet with overlaid text.

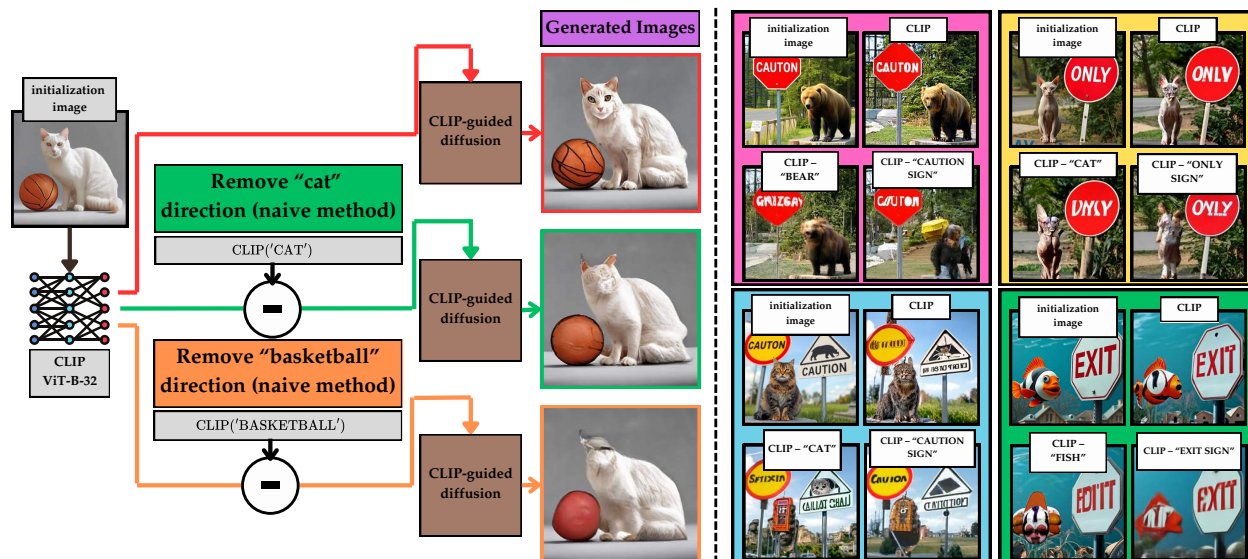


Figure 22: CLIP-guided diffusion process with Naive text embedding cancellation. Starting from an 'initialization image,' generation is guided by CLIP embeddings. The baseline (red arrow) shows unchanged denoising. Naive adjusted CLIP-guided results (green and orange arrows) show image embeddings after subtracting the text CLIP embedding.

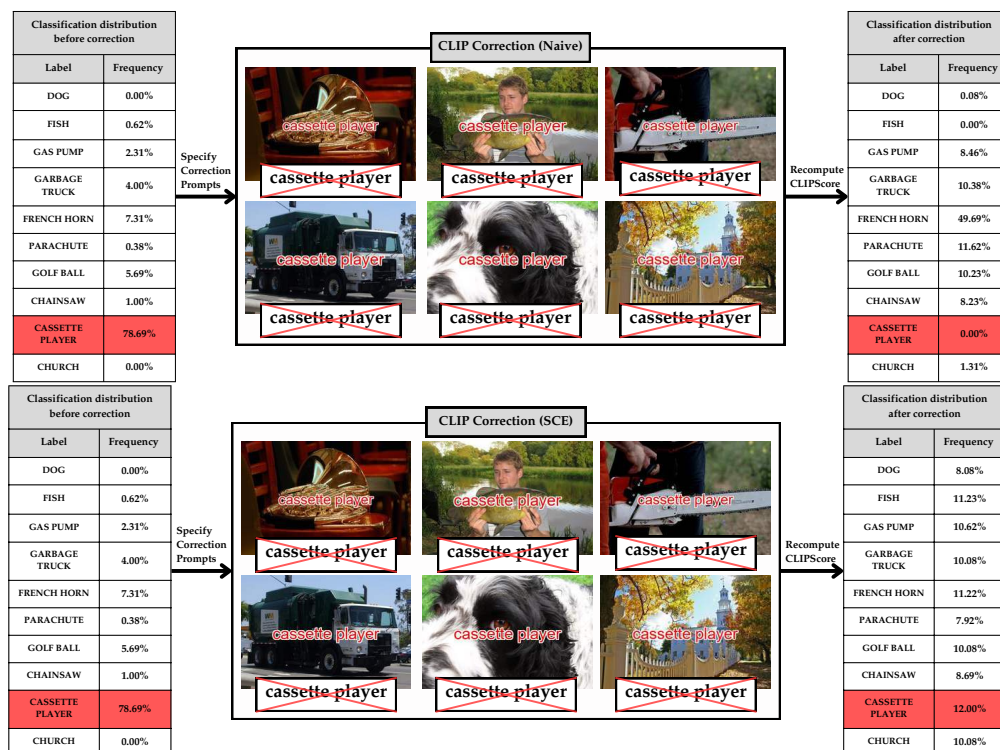


Figure 23: Effect of removing encoded "cassette player" text on top of ImageNet samples. Top figure represents naive method and bottom figure represents SC method.



Figure 24: Comparison of samples generated by naive and SC-based decompositions of CLIP.

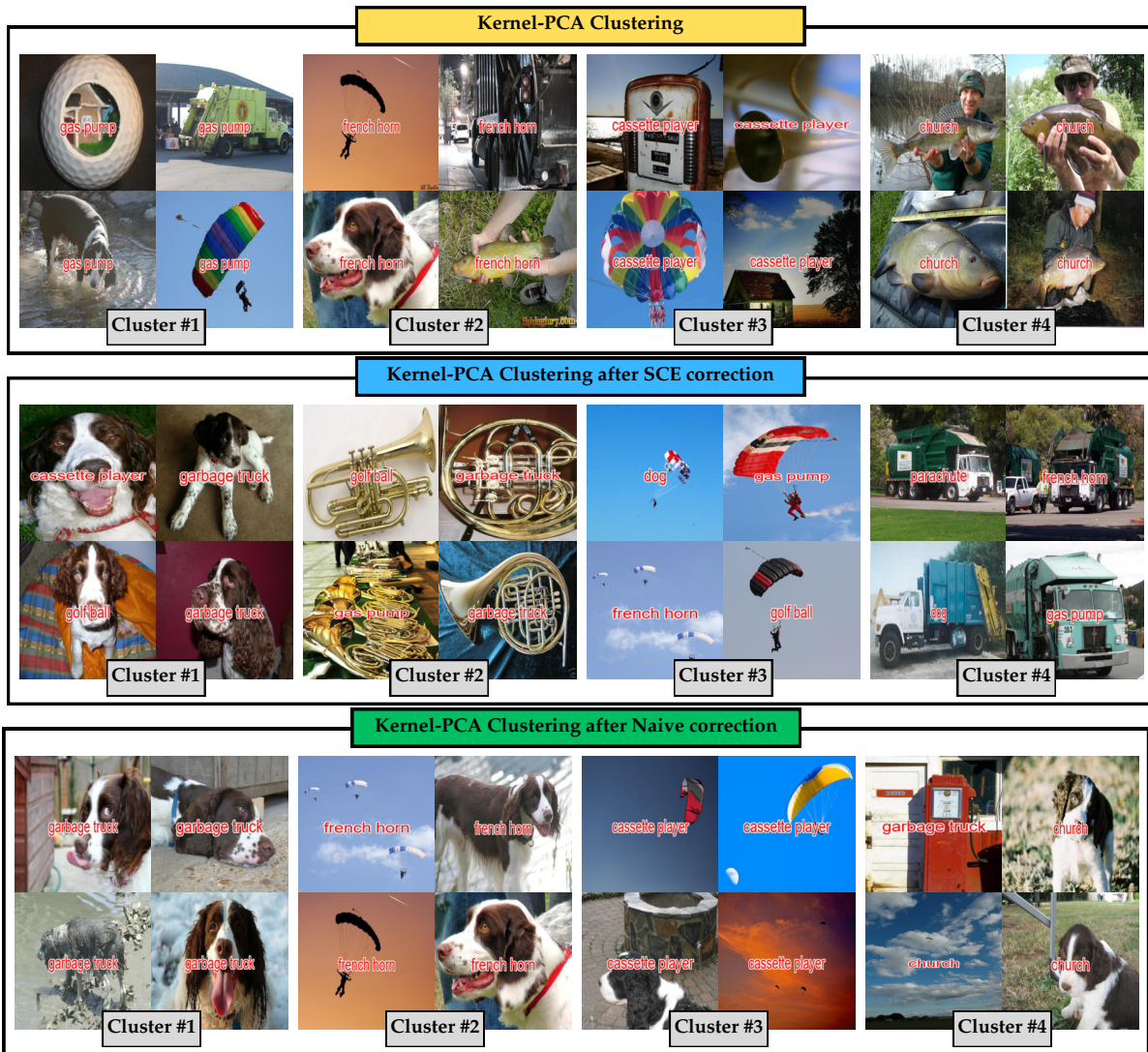


Figure 25: Kernel PCA clusters before and after CLIP correction on the captioned ImageNet dataset, comparing the SCE decomposition approach with the naive approach.

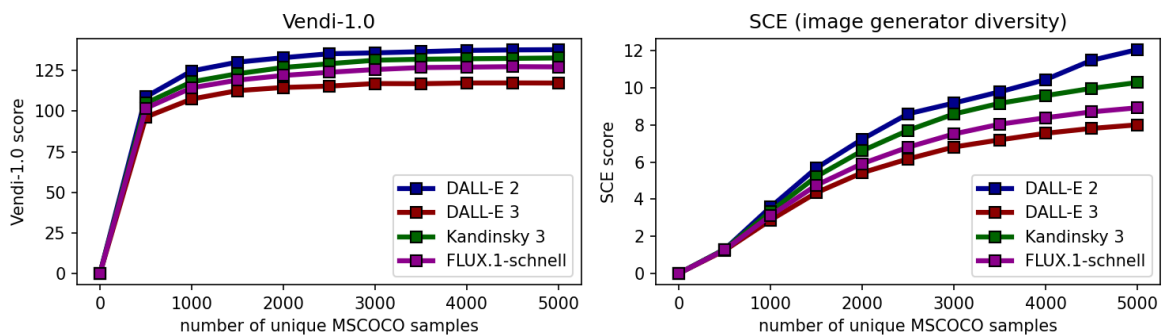


Figure 26: Comparison of different text-to-image models with Vendi-1.0 (generated image diversity) and SCE (image generator diversity).